PART I

A SECOND APPROXIMATION TO THE INDUCED DRAG OF A HELICOPTER ROTOR IN FORWARD FLIGHT

PART II

THE INSTANTANEOUS INDUCED VELOCITY AT THE BLADE OF A FINITE-BLADED ROTOR IN FORWARD FLIGHT

Thesis By

Raymond W. Prouty

In Partial Fulfillment of the Requirements

For the Degree of

Aeronautical Engineer

California Institute of Technology

Pasadena, California

1958

ABSTRACT

In Part I, a method is derived for determining the induced drag of a helicopter rotor in forward flight from the distribution of circulation in the wake. Charts of the correction factor to be applied to the ordinary momentum value of induced drag are presented for ranges of flight parameters currently in use.

In Part II, the expression for the instantaneous induced velocity at a blade is developed by application of the Biot and Savart Law to a helical wake surface on which the circulation distribution varies both with radius and with azimuth in a manner corresponding to the actual lift distribution on the blade.

ACKNOWLEDGEMENT

I wish to express my gratitude to my advisor, Dr. H. J. Stewart, who contributed many helpful suggestions concerning the fundamental concepts used in this work; to Dr. R. Nathan and the California Institute of Technology Computing Center for permission to use the digital computer; and to my typist, Miss Joyce Hoffman, who made her work a labor of love.

TABLE OF CONTENTS

I. A SECOND APPROXIMATION TO THE INDUCED DRAG OF A HELICOPTER ROTOR IN FORWARD FLIGHT

A. SUMMARY

A method is presented for computing the induced drag of a helicopter rotor at forward speeds for which the wake may be considered to form a vortex sheet. The method has been used to compute the induced drag for ranges of twist, tip speed ratio, inflow ratio, and thrust coefficient/solidity ratio currently in use. The results are presented on charts as the ratio between the induced drag computed by this method and the induced drag computed by the momentum equation. The computed induced drag ratio varies from 1.14 to 7.90, with the latter value corresponding to a highly twisted, lightly loaded rotor at a high tip speed ratio.

B. INTRODUCTION

In those methods for estimating forward flight performance based on balance of energy, the induced drag--or induced power--is evaluated from a momentum equation involving the rotor thrust and the uniform downward acceleration of the mass of air contained in a streamtube with diameter equal to that of the rotor. For the case in which the induced velocity is negligible compared with the forward velocity, the momentum equation for induced drag is:

$$D_i = \frac{T^2}{2\rho A V^2} \tag{1}$$

This concept was originally developed for wings and was first applied to rotors by Glauert during his study of autogyros. In this paper it is considered to be the first approximation inferred in the title.

That the first approximation is likely to give optimistic results is apparent upon considering that for wings it applies strictly only to an elliptical spanwise lift distribution which may be shown to be the case for minimum induced drag. Thus it is to be expected that if a rotor does not correspond to a wing with elliptical lift distribution, the induced drag will be higher than the value computed from the momentum equation.

C. SYMBOLS

A Rotor disc area, sq ft

AR Wing aspect ratio

a Slope of lift curve, C_L/radian = 5.73

a_o Steady blade flapping angle, radians

a_1 Longitudinal angle between a plane normal to the control axis and the tip path plane, radians

B_m Fourier sine coefficient of distribution of C in the remote wake

b Wing span, ft--Number of rotor blades

C_L Coefficient of lift = $\frac{L}{qS}$

C_Γ Coefficient of circulation = $\frac{\Gamma}{\frac{\Omega R c a b}{4\mu\pi}}$

C_T/σ Thrust coefficient/solidity ratio = $\frac{T}{\rho A \sigma (\Omega R)^2}$

c Chord of rotor blade, ft

D Perpendicular distance between point and vortex element

D_i Induced drag, lbs

D_{i_M} Induced drag computed by momentum equation, lbs

F Tip loss function = F(r/R)

h Distance between point and vortex element

L Lift, lbs

q Dynamic pressure, lbs/sq ft--General velocity, ft/sec

R Rotor radius, ft

R_e Radius outboard of which no lift is developed, ft

R_o Radius inboard of which no lift is developed, ft

r Radius to blade element, ft

S Wing area, sq ft

T Rotor thrust, lbs

t Distance along vortex element, ft

U_T Tangential velocity at blade element, ft/sec

V Forward velocity, ft/sec

w Vertical component of induced velocity, ft/sec

$\overline{w}$ Average vertical component of induced velocity, obtained from momentum equation, ft/sec

X, Y, Z Cartesian coordinates

α Angle of attack of blade element, radians; Angle of attack of control plane, radians

$-\alpha_s$ Negative stalling angle of attack for blade element in reversed flow region

Γ Circulation, ft^2/sec

γ Vorticity, radians/sec

$1+\delta$ Induced drag ratio $= \frac{D_i}{D_{i_M}}$

η Independent variable across wake ($\cos\eta = y/R$)

θ_o Collective pitch, radians

θ_1 Rotor blade twist, radians

λ Inflow ratio

μ Tip speed ratio

ξ Accumulative wake azimuth angle, radians

ρ Density of air, slugs/cu ft

σ Rotor solidity $= \frac{bc}{\pi R}$

ψ Rotor blade azimuth position, radians

Ω Rotor angular velocity, radians/sec

Subscripts:

e Blade element

w Wake

a Advancing

r Retreating

Sub-subscripts:

N Normal flow

R Reverse flow

D. ANALYSIS

1. The Induced Drag of a Wing:

Before discussing the induced drag of a rotor, it will be fruitful to review some of the factors concerning the induced drag of a wing. A wing with an arbitrary lift distribution is shown in Figure 1. The wake consists of a vortex sheet with a distribution of circulation corresponding to the distribution of lift on the wing. The entire vortex sheet induces velocities, q, in the air surrounding the wake and the kinetic energy corresponding to these induced velocities is related to the induced drag of the wing. More specifically, at a point in the remote wake sufficiently downstream to be unaffected by the bound vortex at the wing, the kinetic energy--in foot pounds--contained in a cell one foot thick in the direction of flight and extending to infinity in the Y and Z directions is numerically equal to the induced drag--in pounds--of the wing. Thus the induced drag is:

$$D_i = \text{K.E./ ft.} = \int_{x=x_1}^{x_1+1} \int_{y=-\infty}^{\infty} \int_{z=-\infty}^{\infty} \frac{1}{2} \rho q^2 \, dx \, dy \, dz \qquad (2)$$

It may be shown that this triple integral reduces to a single integral over the span of the wake:

$$D_i = \rho \int_{-\frac{b}{2}}^{\frac{b}{2}} w(y) \, \Gamma(y) \, dy \qquad (3)$$

where w(y) and $\Gamma(y)$ are the vertical component of induced velocity and the

circulation distribution respectively at the surface of the vortex sheet. If $\Gamma(y)$ is elliptical, w(y) will be constant and the induced drag will not only be a minimum, but will be the same as obtained from the momentum equation. In coefficient form this case gives the equation familiar to all aerodynamicists:

$$C_{D_i} = \frac{C_L^2}{\pi AR} \tag{4}$$

Equation 3 can be derived by considering conditions at the wing itself as shown by Von Mises in Reference 1, but by indicating that it can also be derived from the remote wake without considering the agency which produced the wake, the possibility of applying the method to rotors becomes evident.

2. The Wake of a Rotor in Forward Flight:

To develop an understanding of the wake of a rotor, it is convenient to think of a rotor moving through still air and depositing its wake as it flies past the observer. It will be assumed that the induced velocity is negligible compared to the forward velocity so that the wake stays in the plane of the rotor. A corollary assumption is that the tendency of the remote wake to roll up into two vortices may be ignored. For the purposes of this analysis, these assumptions are thought to be valid at the cruising speed and above of all current helicopters.

The quantity deposited by each blade element in forming the wake is circulation and the strength of the wake at any point is equal to the circulation on the blade element--or blade elements--as it passed that point. This blade elemental circulation, Γ_e, is a function of the lift of the blade element as

expressed by the equation:

$$dL = \rho U_T \Gamma_e \, dr \tag{5}$$

but dL is related to the angle of attack, chord, slope of the lift curve, and tangential velocity:

$$dL = \frac{\rho}{2} U_T^2 \, a \, \alpha c \, dr \tag{6}$$

Thus:

$$\Gamma_e = \frac{U_T}{2} c a \alpha \tag{7}$$

The tangential velocity is a function of rotor speed, tip speed ratio, and azimuth such that:

$$\Gamma_e = \frac{\Omega R c a}{2} \left(\frac{r}{R} + \mu \sin \psi \right) \alpha \tag{8}$$

At this point, it is necessary to distinguish between the blade element circulation in normal flow and in reversed flow since for most helicopter flight conditions, the reversed flow region is stalled negatively and the lift is not proportional to the angle of attack. Sub-subscripts N and R will be used on Γ_e to distinguish these two regions. For the normal flow region, the angle of attack of the blade element consists of four types of terms: pitch, induced angles, products of flapping and rotational speeds, and products of flapping and forward speeds. Using the notation of Bailey in Reference 2

and neglecting flapping above the first harmonic, Equation 8 expands to:

$$\Gamma_{e_N} = \frac{\Omega R c a}{2}\left[\theta_0 \frac{r}{R} + \theta_1 \left(\frac{r}{R}\right)^2 + \lambda + \left(\theta_0 \mu + \frac{r}{R}\mu\theta_1 - \frac{r}{R}a_1\right)\sin\psi + \left(\frac{r}{R}b_1 - \mu a_0\right)\cos\psi + \mu a_1 \cos^2\psi + \mu b_1 \sin\psi\cos\psi\right] \tag{9}$$

Note that the use of the inflow ratio, λ, in the manner of Reference 2 implies a constant value of induced velocity across the rotor disc. Accounting for a variation of induced velocity would constitute a third approximation to induced drag and will not be attempted in this paper.

In the reversed flow region, it will be assumed that the angle of attack is constant and equal to the negative stalling angle of the airfoil going backward. Thus:

$$\Gamma_{e_R} = \frac{\Omega R c a}{2}\left(-\alpha_s\right)\left(\frac{r}{R} + \mu \sin\psi\right) \tag{10}$$

Equations 9 and 10 define the instantaneous circulation for any blade element and the amount of circulation deposited by that blade element in the wake. Since circulation is a scaler quantity, the circulation at a point in the wake which is affected by more than one blade element is simply the algebraic sum of the circulation of the various blade elements. Figure 2a is a sketch of the circulation in the wake of a single-bladed rotor for a tip speed ratio of about .2. This wake differs from that of a wing by possessing a variation in circulation in the X direction as well as in the Y direction. If the same lift is shared by two blades, however, the streamwise variation is smoothed out as shown in Figure 2b. Extending this procedure to an infinite number of blades completely eliminates the streamwise variation and produces the wake of Figure 2c which might have been generated by a

wing. It is for this infinite-bladed rotor that the analysis will be developed. Note that because the wake of the infinite-bladed rotor has no streamwise variation, the induced velocity at the rotor is steady with time, and that this condition is also a basic assumption of the momentum equation for induced drag. Thus the first and second approximations correspond on this point and differ only in the type of circulation distribution used.

3. Determination of the Distribution of Circulation:

The determination of the distribution of circulation in the wake of an infinite-bladed rotor will be based on the understanding that the analysis of a single blade for a complete revolution is equivalent to the instantaneous analysis of an infinite number of blades. Figure 3 shows the path of a single blade during one revolution. Each blade element traces out a cycloid whose parametric equations are:

$$x = r\cos\psi - \mu R\psi \tag{11}$$

and

$$y = r\sin\psi \tag{12}$$

The circulation in the wake for any value of y is equal to the blade elemental circulation along y integrated with respect to x across the cycloid from front to rear, and to account for overlapping, divided by the distance the entire rotor moves during one revolution, $2\mu R\pi$. Since the distribution with respect to y is desired, Equation 12 may be used to eliminate r from Equations 9 and 10, giving:

$$\Gamma_{e_N} = \frac{\Omega R c a}{2}\left[\theta_o \frac{\frac{y}{R}}{\sin\psi} - \frac{\theta_1 \left(\frac{y}{R}\right)^2}{\sin^2\psi} + \lambda + \theta_o \mu \sin\psi + \frac{y}{R}\mu\theta_1 - \frac{y}{R}a_1\right.$$

$$\left. + \frac{y}{R} b_1 \cot\psi - \mu a_o \cos\psi + \mu a_1 \cos^2\psi + \mu b_1 \sin\psi\cos\psi\right] \qquad (13)$$

and

$$\Gamma_{e_R} = \frac{\Omega R c a}{2}(-\alpha_s)\left(\frac{\frac{y}{R}}{\sin\psi} + \mu\sin\psi\right) \qquad (14)$$

Before performing the integration, it is necessary to discuss tip and root losses. Two requirements are involved--first: the analysis should correspond in its treatment of tip loss to previous analyses, such as Reference 2, which may be used to compute θ_o and a_1 for actual cases; and secondly, discontinuities (infinite slopes) in the circulation distribution, which may be shown to lead to infinite induced drag, must be avoided. The first requirement is satisfied by assuming--as in Reference 2--that the portion of the blade outboard of an effective radius, R_e, contributes no lift. The second requirement is automatically satisfied at the edges of the wake by the "scalloped" effect of the single-bladed cycloid as shown in Figures 2a and 3; e.g. even if the circulation is finite at R_e, the integration on x for $y = \pm R_e$ is for an infinitesimal length and produces zero values for the circulation at the edges of the wake of the infinite-bladed rotor. At the root, the second requirement is not automatically satisfied. Equations 13 and 14 show that the circulation at y = 0 has one value during the advancing half-cycle and another value during the retreating half-cycle. Thus the

integration with respect to x at y = 0 yields two values of circulation--or a discontinuity. This discontinuity may easily be removed by assuming that no circulation is generated by the portion of the blade inboard of an effective root radius, R_o. As may be seen from Figure 3, this has the same scalloping effect as that which prevented infinite slopes at the edges of the wake. A survey of current helicopter rotors shows that the actual airfoil section begins 7% to 24% of the rotor radius from the center of rotation. It is felt that to this should be added the 3% inboard portion of the airfoil section to allow for the falling off of the lift. On this basis, an effective root radius may be determined for a given rotor with a value of about 10% of the rotor radius taken as a minimum.

For purposes of integration, the single-blade cycloid of Figure 3 may be divided into streamwise zones which are distinguished by the combination of normal flow, reversed flow, tip loss, and root loss which they contain. The zones and their limits are tabulated below.

Zone	Normal Flow	Reversed Flow	Tip Loss	Root Loss	Limits
I			X		$R_e < y < R$
II	X		X		$R_o < y < R_e$
III	X		X	X	$0 < y < R_o$
IV	X		X	X	$\frac{-R_o^2}{\mu R} < y < 0$
V	X	X	X	X	$-R_o < y < \frac{-R_o^2}{\mu R}$
VI	X	X	X		$-\mu R < y < -R_o$
VII	X		X		$-R_e < y < -\mu R$
VIII			X		$-R < y < -R_e$

Note: If $\frac{R_o}{R} \geq \mu$, Zones IV, V, and VI combine into one.

The zones are shown on Figure 3 both on the cycloid corresponding to fixed axes and on the disc corresponding to moving axes. Each zone has its own integration procedure and limits of integration. In Figure 3, the limits for two values of y are shown: one on the advancing side where a is used as a subscript, and one on the retreating side where r is used. The limits occur in pairs (for example, d_a and e_a, h_r and i_r) for which the alphabetical order has been made to correspond to increasing ψ during the rotation of the blade. The integration of elemental circulation for constant values of y divided by the distance the rotor travels in one revolution, $2\mu R\pi$, produces the circulation in the wake of the infinite-bladed rotor, Γ_w. For the various zones, the integrations are:

Zone I

$$\Gamma_w^{I} = 0 \tag{15}$$

Zone II

$$\Gamma_w^{II} = \frac{1}{2\mu R\pi}\left[-\int_{d_a}^{e_a} \Gamma_{e_N}\, dx\right] \tag{16}$$

Zone III

$$\Gamma_w^{III} = \frac{1}{2\mu R\pi}\left[-\int_{d_a}^{e_a} \Gamma_{e_N}\, dx + \int_{f_a}^{g_a} \Gamma_{e_N}\, dx\right] \tag{17}$$

Zone IV

$$\Gamma_w^{IV} = \frac{1}{2\mu R\pi}\left[\int_{d_r}^{e_r} \Gamma_{e_N}\, dx - \int_{f_r}^{g_r} \Gamma_{e_N}\, dx\right] \tag{18}$$

Zone V

$$\Gamma_w^{V} = \frac{1}{2\mu R\pi}\left[\int_{d_r}^{e_r} \Gamma_{e_N}\, dx - \int_{h_r}^{i_r} \Gamma_{e_N}\, dx - \int_{h_r}^{i_r} \Gamma_{e_R}\, dx + \int_{f_r}^{g_r} \Gamma_{e_R}\, dx\right] \tag{19}$$

Zone VI

$$\Gamma_w^{VI} = \frac{1}{2\mu R\pi}\left[\int_{d_r}^{e_r}\Gamma_{e_N}\,dx - \int_{h_r}^{i_r}\Gamma_{e_N}\,dx - \int_{h_r}^{i_r}\Gamma_{e_R}\,dx\right] \tag{20}$$

Zone VII

$$\Gamma_w^{VII} = \frac{1}{2\mu R\pi}\left[\int_{d_r}^{e_r}\Gamma_{e_N}\,dx\right] \tag{21}$$

Zone VIII

$$\Gamma_w^{VIII} = 0 \tag{22}$$

Solving for x as a function of y from the parametric equations of the cycloid, Equations 11 and 12, and differentiating gives:

$$dx = -R\left(\frac{\frac{V}{R}}{\sin^2\psi} + \mu\right)\,d\psi \tag{23}$$

Thus the integrals of Equations 15 to 22 have the form:

$$\int_{x_{\psi_{LO}}}^{x_{\psi_{UP}}}\Gamma_e\,dx = -R\int_{\psi_{LO}}^{\psi_{UP}}\Gamma_e\left(\frac{\frac{V}{R}}{\sin^2\psi} + \mu\right)\,d\psi \tag{24}$$

where Γ_e is given by Equation 13 or 14.

The integration is easily carried out with the use of standard tables of integrals. During substitution of the limits, use is made of the fact that the upper and lower limits are symmetrical about $\psi = 90^\circ$ or 270°. The result of the integration is two equations, one for normal flow and one for reversed flow:

$$\int_{x_{\psi_{LO}}}^{x_{\psi_{UP}}} \Gamma_{e_N}\, dx = -\frac{\Lambda R^2 ca}{2}\left\{\left[\left(\lambda\mu+\frac{\mu^2 a_1}{2}\right)+\left(\mu^2\theta_1-2\mu a_1\right)\frac{Y}{R}\right]\left(\psi_{UP}-\psi_{LO}\right)\right.$$

$$+\left[\left(2\lambda+2\mu a_1\right)\frac{Y}{R}+\left(4\mu\theta_1-2a_1\right)\left(\frac{Y}{R}\right)^2+2\theta_1\left(\frac{Y}{R}\right)^3\right]\frac{\cos\psi_{LO}}{\sin\psi_{LO}}$$

$$+\frac{2}{3}\theta_1\left(\frac{Y}{R}\right)^3\frac{\cos^3\psi_{LO}}{\sin^3\psi_{LO}}+\theta_0\left(\frac{Y}{R}\right)^2\frac{\cos\psi_{LO}}{\sin^2\psi_{LO}}+2\theta_0\mu^2\cos\psi_{LO}$$

$$\left.-\mu^2 a_1\sin\psi_{LO}\cos\psi_{LO}+\left[2\theta_0\mu\frac{Y}{R}+\frac{\theta_0}{2}\left(\frac{Y}{R}\right)^2\right]\ln\left|\frac{1+\cos\psi_{LO}}{1-\cos\psi_{LO}}\right|\right\} \tag{25}$$

$$\int_{x_{\psi_{LO}}}^{x_{\psi_{UP}}} \Gamma_{e_R}\, dx = -\left(-\alpha_s\right)\frac{\Lambda R^2 ca}{2}\left\{\left(\frac{Y}{R}\right)^2\frac{\cos\psi_{LO}}{\sin^2\psi_{LO}}+2\mu^2\cos\psi_{LO}\right.$$

$$\left.+\left[\frac{1}{2}\left(\frac{Y}{R}\right)^2+2\mu\frac{Y}{R}\right]\ln\left|\frac{1+\cos\psi_{LO}}{1-\cos\psi_{LO}}\right|\right\} \tag{26}$$

It is of interest to note that b_1 and a_0 drop out of the problem upon substitution of the limits. Since the upper and lower limits of ψ may be written as functions of y, R_e, R_o, and μ for the various zones, Equations 15 to 22 may in principle be evaluated to provide the distribution of circulation in the wake as a function of y. The corresponding distribution of downwash may then be calculated and Equation 3 evaluated for induced drag. A more convenient computing procedure, however, is outlined in Reference 1 and makes use of a Fourier sine analysis of the distribution of circulation. To use this procedure, a transformation is used:

$$\frac{Y}{R} = \cos\eta \tag{27}$$

This transformation places the advancing tip at $\eta = 0$, the retreating tip at $\eta = \pi$, and converts an elliptical distribution into half a sine wave. The functions of ψ_{io} and ψ_{up} which are required in Equations 25 and 26 are:

$$\psi_{e_a} - \psi_{d_a} = \pi - 2 \sin^{-1}\left(\frac{R}{R_e} \cos\eta\right) \tag{28}$$

$$\psi_{g_a} - \psi_{f_a} = \pi - 2 \sin^{-1}\left(\frac{R}{R_o} \cos\eta\right) \tag{29}$$

$$\psi_{e_r} - \psi_{d_r} = \pi + 2 \sin^{-1}\left(\frac{R}{R_e} \cos\eta\right) \tag{30}$$

$$\psi_{g_r} - \psi_{f_r} = \pi + 2 \sin^{-1}\left(\frac{R}{R_o} \cos\eta\right) \tag{31}$$

$$\psi_{i_r} - \psi_{h_r} = \pi - 2 \sin^{-1}\sqrt{\frac{-\cos\eta}{\mu}} \tag{32}$$

$$\sin \psi_{d_a} = \frac{R}{R_e} \cos\eta \tag{33}$$

$$\cos \psi_{d_a} = \sqrt{1 - \left(\frac{R}{R_e}\right)^2 \cos^2\eta} \tag{34}$$

$$\sin \psi_{f_a} = \frac{R}{R_o} \cos\eta \tag{35}$$

$$\cos \psi_{f_a} = \sqrt{1 - \left(\frac{R}{R_o}\right)^2 \cos^2\eta} \tag{36}$$

$$\sin \psi_{d_r} = \frac{R}{R_e} \cos\eta \tag{37}$$

$$\cos \psi_{d_r} = -\sqrt{1 - \left(\frac{R}{R_e}\right)^2 \cos^2\eta} \tag{38}$$

$$\sin \psi_{f_r} = \frac{R}{R_o} \cos\eta \tag{39}$$

$$\cos \psi_{f_r} = -\sqrt{1 - \left(\frac{R}{R_o}\right)^2 \cos^2 m} \tag{40}$$

$$\sin \psi_{h_r} = -\sqrt{\frac{-\cos m}{\mu}} \tag{41}$$

$$\cos \psi_{h_r} = -\sqrt{1 + \frac{\cos m}{\mu}} \tag{42}$$

The various integrals which appear in Equations 15 to 22 may now be written as functions of m using Equation 27 and Equations 28 to 42. After the necessary algebra is performed, the resulting integrals are:

$$-\int_{d_a}^{e_a} \Gamma_{e_N} dx = \frac{\Lambda R^2 c a}{2} \left\{ \left[C_1 + C_2 \cos m\right]\left[\pi - 2 \sin^{-1}\left(\frac{R}{R_e} \cos m\right)\right] + \left[C_3 + C_4 \cos m + C_5 \cos^2 m\right] \sqrt{1 - \left(\frac{R}{R_e}\right)^2 \cos^2 m} + \left[C_6 \cos m + C_7 \cos^2 m\right] \ln \left| \frac{1 + \sqrt{1 - \left(\frac{R}{R_e}\right)^2 \cos^2 m}}{1 - \sqrt{1 - \left(\frac{R}{R_e}\right)^2 \cos^2 m}} \right| \right\} \tag{43}$$

$$\int_{r_a}^{q_a} \Gamma_{e_N} dx = -\frac{\Lambda R^2 c a}{2} \left\{ \left[C_1 + C_2 \cos m\right]\left[\pi - 2 \sin^{-1}\left(\frac{R}{R_o} \cos m\right)\right] + \left[C_8 + C_9 \cos m + C_{10} \cos^2 m\right] \sqrt{1 - \left(\frac{R}{R_o}\right)^2 \cos^2 m} + \left[C_6 \cos m + C_7 \cos^2 m\right] \ln \left| \frac{1 + \sqrt{1 - \left(\frac{R}{R_o}\right)^2 \cos^2 m}}{1 - \sqrt{1 - \left(\frac{R}{R_o}\right)^2 \cos^2 m}} \right| \right\} \tag{44}$$

$$\int_{d_r}^{e_r} \Gamma_{e_N}\, dx = \frac{\Omega R^2 c a}{2}\left\{\left[C_1+C_2\cos\eta\right]\left[-\pi-2\sin^{-1}\left(\frac{R}{R_e}\cos\eta\right)\right]\right.$$

$$+\left[C_3+C_4\cos\eta+C_5\cos^2\eta\right]\sqrt{1-\left(\frac{R}{R_e}\right)^2\cos^2\eta}$$

$$\left.+\left[C_6\cos\eta+C_7\cos^2\eta\right]\ln\left|\frac{1+\sqrt{1-\left(\frac{R}{R_e}\right)^2\cos^2\eta}}{1-\sqrt{1-\left(\frac{R}{R_e}\right)^2\cos^2\eta}}\right|\right\} \qquad (45)$$

$$-\int_{f_r}^{g_r} \Gamma_{e_N}\, dx = -\frac{\Omega R^2 c a}{2}\left\{\left[C_1+C_2\cos\eta\right]\left[-\pi-2\sin^{-1}\frac{R}{R_o}\cos\eta\right]\right.$$

$$+\left[C_8+C_9\cos\eta+C_{10}\cos^2\eta\right]\sqrt{1-\left(\frac{R}{R_o}\right)^2\cos^2\eta}$$

$$\left.+\left[C_6\cos\eta+C_7\cos^2\eta\right]\ln\left|\frac{1+\sqrt{1-\left(\frac{R}{R_o}\right)^2\cos^2\eta}}{1-\sqrt{1-\left(\frac{R}{R_o}\right)^2\cos^2\eta}}\right|\right\} \qquad (46)$$

$$-\int_{h_r}^{i_r} \Gamma_{e_N}\, dx = \frac{\Omega R^2 c a}{2}\left\{\left[C_1+C_2\cos\eta\right]\left[\pi-2\sin^{-1}\sqrt{\frac{-\cos\eta}{\mu}}\right]\right.$$

$$+\left[C_{11}\cos\eta+C_{12}\cos^2\eta+C_{13}\cos^3\eta\right]\left[\frac{\sqrt{1+\frac{\cos\eta}{\mu}}}{\sqrt{\frac{-\cos\eta}{\mu}}}\right]$$

$$+C_{14}\cos^3\eta\left[\frac{\sqrt{1+\frac{\cos\eta}{\mu}}}{\sqrt{\frac{-\cos\eta}{\mu}}}\right]^3+\left[C_{15}+C_{16}\cos\eta\right]\sqrt{1+\frac{\cos\eta}{\mu}}$$

$$\left.+C_{17}\sqrt{\frac{-\cos\eta}{\mu}}\sqrt{1+\frac{\cos\eta}{\mu}}-\left[C_6\cos\eta+C_7\cos^2\eta\right]\ln\left|\frac{1+\sqrt{1+\frac{\cos\eta}{\mu}}}{1-\sqrt{1+\frac{\cos\eta}{\mu}}}\right|\right\} \qquad (47)$$

$$-\int_{h_r}^{i_r} \Gamma_{e_R}\, dx = \frac{\Omega R^2 c a}{2}\left\{\left[C_{18}+C_{19}\cos\eta\right]\sqrt{1+\frac{\cos\eta}{\mu}}\right.$$

$$\left.+\left[C_{20}\cos\eta+C_{21}\cos^2\eta\right]\ln\left|\frac{1+\sqrt{1+\frac{\cos\eta}{\mu}}}{1-\sqrt{1+\frac{\cos\eta}{\mu}}}\right|\right\} \tag{48}$$

$$\int_{f_r}^{g_r} \Gamma_{e_R}\, dx = -\frac{\Omega R^2 c a}{2}\left\{C_{22}\sqrt{1-\left(\frac{R}{R_o}\right)^2\cos^2\eta}\right.$$

$$\left.+\left[C_{20}\cos\eta+C_{21}\cos^2\eta\right]\ln\left|\frac{1+\sqrt{1-\left(\frac{R}{R_o}\right)^2\cos^2\eta}}{1-\sqrt{1-\left(\frac{R}{R_o}\right)^2\cos^2\eta}}\right|\right\} \tag{49}$$

where:

$$C_1 = \lambda\mu + \frac{\mu^2 a_1}{2} \tag{50}$$

$$C_2 = \mu^2\theta_1 - 2\mu a_1 \tag{51}$$

$$C_3 = 2\lambda\frac{R_e}{R} + 2\mu a_1\frac{R_e}{R} + \frac{2}{3}\theta_1\left(\frac{R_e}{R}\right)^3 + \theta_o\left(\frac{R_e}{R}\right)^2 + 2\theta_o\mu^2 \tag{52}$$

$$C_4 = 4\mu\theta_1\frac{R_e}{R} - 2a_1\frac{R_e}{R} - \mu^2 a_1\frac{R}{R_e} \tag{53}$$

$$C_5 = \frac{4}{3}\theta_1\frac{R_e}{R} \tag{54}$$

$$C_6 = 2\theta_o\mu \tag{55}$$

$$C_7 = \frac{\theta_o}{2} \tag{56}$$

$$C_8 = 2\lambda\frac{R_o}{R} + 2\mu a_1\frac{R_o}{R} + \frac{2}{3}\theta_1\left(\frac{R_o}{R}\right)^3 + \theta_o\left(\frac{R_o}{R}\right)^2 + 2\theta_o\mu^2 \tag{57}$$

$$C_9 = 4\mu\theta_1 \frac{R_o}{R} - 2a_1 \frac{R_o}{R} - \mu^2 a_1 \frac{R}{R_o} \tag{58}$$

$$C_{10} = \frac{4}{3}\theta_1 \frac{R_o}{R} \tag{59}$$

$$C_{11} = 2\lambda + 2\mu a_1 \tag{60}$$

$$C_{12} = 4\mu\theta_1 - 2a_1 \tag{61}$$

$$C_{13} = 2\theta_1 \tag{62}$$

$$C_{14} = \frac{2}{3}\theta_1 \tag{63}$$

$$C_{15} = -2\theta_o\mu^2 \tag{64}$$

$$C_{16} = \theta_o\mu \tag{65}$$

$$C_{17} = -\mu^2 a_1 \tag{66}$$

$$C_{18} = -2\mu^2(-\alpha_s) \tag{67}$$

$$C_{19} = \mu(-\alpha_s) \tag{68}$$

$$C_{20} = -2\mu(-\alpha_s) \tag{69}$$

$$C_{21} = -\frac{1}{2}(-\alpha_s) \tag{70}$$

$$C_{22} = \left[-2\mu^2 - \left(\frac{R_o}{R}\right)^2\right](-\alpha_s) \tag{71}$$

The distribution of Γ_w as a function of m may now be determined using Equations 15 to 22, 43 to 49, and 50 to 71. At this point it is convenient to introduce a non-dimensional coefficient of circulation, $C_\Gamma(m)$, which will be defined by the equation:

$$\Gamma_w(m) = \frac{\Omega R c a b}{4\mu\pi} C_\Gamma(m) \tag{72}$$

where the multiplier is the product of the multipliers in Equations 16 and 43 and the number of blades, b. Up to this point, the derivation has made use of only one blade, but it is clear that in principle any number could have been used. The coefficient of circulation consists of sums of the quantities within the brackets in Equations 43 to 49. For any value of m the coefficient is a function of μ, λ, θ_0, a_1, θ_1, R_e/R, R_0/R, and $(-\alpha_s)$ or since θ_0 and a_1 are functions of μ, λ, θ_1, and C_T/σ, the parameters may be taken as μ, λ, C_T/σ, θ_1, R_e/R, R_0/R, and $(-\alpha_s)$ where the first three are flight parameters and the last four are physical parameters. Since the coefficient of circulation is of a more general nature than the circulation itself, the Fourier analysis will be made on it.

4. Fourier Analysis of the Coefficient of Circulation:

The Fourier sine series which represents the distribution of $C_\Gamma(m)$ is:

$$C_\Gamma(m) = \sum_{m=1}^{\infty} B_m \sin m m \tag{73}$$

An equation for evaluating the Fourier sine coefficients is given by Whittaker and Robinson in Reference 3:

$$B_m = \frac{2}{n}\left[C_{\Gamma_1}\sin\frac{m\pi}{n} + C_{\Gamma_2}\sin\frac{2m\pi}{n} + C_{\Gamma_3}\sin\frac{3m\pi}{n} + \cdots C_{\Gamma_{n-1}}\sin\frac{(n-1)m\pi}{n}\right] \tag{74}$$

where n is the number of intervals into which the half-period, 0 to π, is divided and C_{Γ_i} is the value of C_Γ at the upper boundary of each interval.

The Fourier sine coefficients may now be used to evaluate the ratio between the induced drag corresponding to the computed circulation distribution and the induced drag found by the momentum equation. According to Reference 1 this ratio is:

$$\frac{D_i}{D_{i_M}} = (1+\delta) = \sum_{m=1}^{\infty} \frac{m B_m^2}{B_1^2} \tag{75}$$

In practice only a finite number of the coefficients can be evaluated, but unless the circulation distribution contains discontinuities, the contributions of the higher harmonics become very small and the series converges. If a discontinuity exists in the distribution, the contributions of the higher harmonics will not become small and the series will not converge, but will give a value of induced drag of infinity. It was precisely to avoid this possibility that root loss was included in the derivation. Without consideration of root loss, the circulation at the center of rotation will be one value as the blade advances and another as it retreats, thus producing a discontinuity down the center of the wake.

The Fourier coefficients represent not only the induced drag, but the rotor thrust and the rolling moment as well. The thrust may be obtained from the same equation which gives the lift of a wing:

$$T = \rho V \int_{-R}^{R} \Gamma_w \, dy \tag{76}$$

where dy may be derived from Equation 27 and Γ_w is given by Equation 72. Combining these equations gives:

$$T = \frac{\rho V \Omega R^2 c a b}{4} \int_0^{\pi} C_l(m) \sin m \, dm \tag{77}$$

If the Fourier series for $C_T(\psi)$ is substituted into Equation 77, all of the harmonics except the first vanish, leaving:

$$T = \rho(\Omega R)^2 R c b a \quad \frac{B_1}{8} \tag{78}$$

which may be rearranged to:

$$B_1 = \frac{8 C_T/\sigma}{a} \tag{79}$$

The Fourier coefficient of the second harmonic, B_2, represents the rolling moment and should be zero for steady flight conditions. These two relationships for the first and second coefficients are useful for checking the computation of actual cases.

E. INDUCED DRAG COMPUTATIONS

1. Computing Program:

The distribution of the circulation coefficient and the corresponding value of the induced drag ratio, $1 + \delta$, has been computed for a total of 82 cases. The first 81 cases include all combinations of the following:

$$\theta_1 = 0^\circ, -8^\circ, \text{ and } -16^\circ$$

$$\mu = .15, .25, .35$$

$$C_T/\sigma = .04, .08, .12$$

$$\lambda = 0, -.05, -.10$$

For these cases, R_e/R was chosen as .97 to correspond to Reference 2; R_o/R was chosen as .10, which is the minimum value for current rotor designs; and $-\alpha_s$ was chosen as -8°, which is thought to be a reasonable value for the negative stalling angle of an airfoil going backward. The 82nd case was used to investigate the effect of increased root loss. For this case:

$$R_o/R = .27 \qquad \theta_1 = -8^\circ$$

$$R_e/R = .97 \qquad \mu = .25$$

$$-\alpha_s = -8^\circ \qquad C_T/\sigma = .08$$

$$\lambda = -.05$$

where R_o/R is the maximum value for current rotor designs.

The values of θ_o and a_1 for use in Equations 50 to 71 were obtained using the equations and tables of Reference 2. The coefficient of circulation was evaluated for 48 values of n and consequently 47 Fourier sine coefficients were obtained for the induced drag series of Equation 75. The actual computing was performed on the Electrodata Datatron digital computer on the campus of the California Institute of Technology.

2. Induced Drag Charts:

Figures 4, 5, and 6 are plots of the computed values of induced drag ratio, $1 + \delta$, for $R_o/R = .10$. These charts may be used to supplement the performance charts of Reference 4 to provide a complete performance estimation method. The values of $1 + \delta$ plotted on the induced drag charts vary from a minimum of 1.143 at $\theta_1 = 0$, $C_T/\sigma = .08$, $\lambda = -.10$, and $\mu = .35$ to a maximum of 7.898 at $\theta_1 = -16^\circ$, $C_T/\sigma = .04$, $\lambda = 0$, and $\mu = .35$. It is interesting to note that the value of $1 + \delta$ for an untapered wing is less than 1.08 for aspect ratios up to 10 as given by Perkins and Hage in Figure 2-44 of Reference 5.

3. Distribution of Circulation Coefficient:

Some typical distributions of the coefficient of circulation are shown in Figures 7 to 10. In these figures, the distribution for $\theta_1 = -8^\circ$, $C_T/\sigma = .08$, $\lambda = -.05$, and $\mu = .25$ has been adopted as a standard and the effect of changing each of the basic variables from this standard is shown. In each figure an ideal elliptical distribution based on the first Fourier coefficient, B_1, is included for comparison. The distributions of the cases of maximum and minimum induced drag ratios computed are shown in Figure 11. The maximum case represents a highly twisted ($\theta_1 = -16^\circ$), lightly loaded ($C_T/\sigma = .04$) rotor at a high tip speed ratio ($\mu = .35$) in the gyrodyne configuration ($\lambda = 0$). For this case the angle of attack at the advancing tip is -4°. A study of the convergence of the induced drag series for this case is summarized in Figure 12 where it may be seen that the first 20 terms account for 96% of the total for 47 terms.

In Figure 13, the distributions for root losses of 10% and 27% are plotted. In addition, the discontinuity due to neglecting the root loss

and which results in an infinite computed induced drag is shown. For the case chosen for this investigation, the induced drag corresponding to $R_o/R = .27$ is 10% higher than for $R_o/R = .10$. This 10% difference does not seem to warrant the preparation of induced charts for root losses other than .10 at this time.

4. The First and Second Computed Fourier Sine Coefficients:

During the derivation of the method, it was pointed out that the first and second Fourier coefficients represent thrust and rolling moment respectively. In particular B_1 should satisfy Equation 79 and B_2 should be zero. For the 81 cases with $R_o/R = .10$, the computed value of B_1 actually varied between 96.5% and 118.1% of the value given by Equation 79, with the minimum value corresponding to $\theta_1 = -16^\circ$, $C_T/\sigma = .04$, $\lambda = 0$, and $\mu = .25$, and the maximum to $\theta_1 = 0$, $C_T/\sigma = .04$, $\lambda = -.10$, and $\mu = .35$. The variation is due to the fact that the values of θ_o and a_1 for use in Equations 50 to 71 were computed by the method of Reference 2 in which no allowance is made for the possibility that the blade elements in the reversed flow region may be stalled negatively. For this reason, the method of Reference 2 overestimates the down-load on the reversed flow region for most flight conditions, and consequently the computed collective pitch and thrust are slightly high. In this paper, the negative lift in the reversed flow region has been assumed to correspond to -8°--a reasonable value for those cases in which the reversed flow region is actually stalled, such as in the case which gave 118.1% of the estimated value of B_1, but a pessimistic value for unstalled cases.

The second Fourier coefficient varied from -.08% of B_1 for $\theta_1 = 0$, $C_T/\sigma = .04$, $\lambda = -.10$, $\mu = .15$ to -3.95% of B_1 for $\theta_1 = -16^\circ$, $C_T/\sigma = .04$, $\lambda = -.10$, and $\mu = .35$. The negative sign on B_1 signifies a rolling moment toward the advancing tip. Again the primary reason for the non-zero character of B_2 is the treatment of the reversed flow region. In the single case computed for $R_o/R = .27$, the reversed flow region lies entirely within the root loss and B_1 is 97.4% of its estimated value and B_2 is -2.01% of B_1.

5. Illustrative Example:

To illustrate the effect of using the second approximation, the sample performance calculation included in Reference 4 will be used. In this calculation:

$$\theta_1 = -8^\circ$$

$$\mu = .30$$

$$C_T/\sigma = .0515$$

$$\lambda = -.08$$

It will be assumed that $R_o/R = .10$. Using the first approximation to induced drag, as Reference 4 does, and applying the performance extimation method outlined there, a total required rotor power of 371 hp was obtained of which 32 hp was due to induced drag. For use in the second approximation, a cross-plot of Figure 5 at $\mu = .30$ gives a value of 1.50 for $1 + \delta$ at $C_T/\sigma = .0515$ and $\lambda = -.08$. Thus the second approximation to induced power is 48 hp and the total rotor power is 387 hp, an increase of about 4.5%. Had the twist been 0° the increase for the same values of C_T/σ, μ, and λ would have been 2.5% and for -16° twist, 16.0%.

F. EXPRIMENTAL VERIFICATION

There is no known method for directly measuring the induced drag either in flight or in a wind tunnel, but the distribution of circulation can be determined from measurements of flow angularity and velocity in the wake. Such measurements have been made in a wind tunnel by the NACA and are reported by Heyson in Reference 6. Figure 14 has been taken from Figure 52 of that report and shows the measured vorticity distribution in the wake immediately behind the rotor for a case in which the skew angle of the wake was 83.9°, a condition which approaches the basic assumption of this analysis--that the wake stays in the plane of the rotor. To obtain the corresponding distribution of circulation, the distribution of vorticity is first integrated with respect to Z to obtain the equivalent vortex sheet. A running integration from each side then gives the distribution of circulation. This integration has been provided by the NACA in an exchange of correspondence and ispresented in Figure 15 with the distribution computed by the method of this paper.

It may be seen that the correlation is good in the outboard regions but is poor in the center. This defect is thought to be the result of the difficulty of measuring induced velocities near the center of the wake. Indeed, Reference 6 claims an accuracy for these velocities of only $\pm$ 25% of the momentum value of induced velocity. Integration of the experimental circulation distribution to obtain thrust gives a value of 347 lbs., whereas the measured thrust was only 276 lbs.--20% less. The computed circulation distribution agrees with the measured thrust since this thrust was used to obtain C_T/σ for the computation. Considering these points, it is

felt that the experimental results provide a verification of the theory and that further refinement of the experimental technique will provide even better correlation.

G. CONCLUSIONS

The technique for determining induced drag from the distribution of circulation in the wake has been applied to a helicopter and the results compared to those obtained using the simple momentum concept. It has been shown that the momentum equation can be greatly in error for certain flight conditions. A partial verification of the analysis has been obtained from NACA wind tunnel tests of a rotor.

II. THE INSTANTANEOUS INDUCED VELOCITY AT THE BLADE OF A FINITE-BLADED ROTOR IN FORWARD FLIGHT

A. SUMMARY

The Biot and Savart Law has been used to derive the expression for the instantaneous vertical component of induced velocity at a rotor blade induced by a family of helical surfaces of vorticity generated by the individual blades of a rotor. The distribution of circulation on each helix is assumed to vary both with radius and with azimuth corresponding to the lift distribution on the generating blade. The resulting expression has the form of a double integral which must be evaluated by numerical means. The problem is in the process of being set up for a high speed digital computer, but at this writing no results are available.

B. INTRODUCTION

A number of attempts to analytically determine the distribution of induced velocity over a rotor in forward flight have been made in recent years, but because of the inherent complexity of the problem each attempt has been based on simplifying assumptions which throw doubt on the final results. The two most common assumptions which have been used are: 1) the rotor has an infinite number of blades, and; 2) the circulation is constant along the blade and around the azimuth. Several authors have been able to relax one or the other of these assumptions, but never both simultaneously. In Section I. D. 2 of this paper, the distribution of circulation as a function of both radius and azimuth in the wake of a single bladed rotor was developed and this will be used to derive the expression for induced velocity at the blade of a finite-bladed rotor.

C. DERIVATION

1. Position of the Rotor Wake:

In the derivation of induced drag in Part I, it was necessary to assume that the wake remained in the plane of the rotor in order to treat it as a vortex sheet. For the derivation of the induced velocity distribution, this assumption is neither necessary nor desirable. In this case, it will be assumed that the wake forms a helical surface which is swept down by the average vertical induced velocity of the rotor, $\overline{w}$, where:

$$\overline{w} = \frac{T}{2\rho A V} \tag{80}$$

The position of the wake is assumed to be determined by the induced velocity at the rotor, $\overline{w}$, rather than by the induced velocity in the ultimate wake, $2\overline{w}$, on the basis that the wake in the immediate neighborhood of the rotor is dominant in inducing velocities at the blades. The side and plan views of the assumed wake are shown in Figure 16. Note that the tip path plane is taken as the X-Y plane with the origin at the center of revolution when $\psi_1 = 0$.

2. Application of the Biot and Savart Law:

The incremental velocity at any point on a rotor blade induced by an incremental vortex element at any point in the wake may be found from the Biot and Savart Law:

$$dq = \frac{\Gamma}{4\pi} \frac{D}{h^3} dt \tag{81}$$

where h is the actual distance between the vortex element and the point on the blade and D is the perpendicular distance. For the case of circulation

distributed on a surface, the circulation may be resolved into components perpendicular and parallel to the "wake blade" of Figure 16. Equation 81 becomes:

$$dq = \frac{\frac{\partial \Gamma}{\partial \frac{r}{R}} d\frac{r}{R}}{4\pi} \frac{D_r}{h^3} dt_3 + \frac{\frac{\partial \Gamma}{\partial 3} d3}{4\pi} \frac{D_3}{h^3} dt_r + \frac{\Gamma_b}{4\pi} \frac{D_b}{h^3} dt_b \qquad (82)$$

The first term of Equation 82 corresponds to trailing vortices produced by the spanwise variation of circulation, the second to shed vortices produced by the variation of circulation around the azimuth, and the third to the bound vortices of other blades in the case of a multi-bladed rotor.

The geometric relationships which are needed to evaluate the terms in Equation 82 are shown on Figure 17. From this figure, it may be seen that the vertical component of dq is:

$$dw = \frac{\frac{\partial \Gamma}{\partial \frac{r}{R}} d\frac{r}{R}}{4\pi} \frac{D_r'}{h^3} dt_3 + \frac{\frac{\partial \Gamma}{\partial 3} d3}{4\pi} \frac{D_3'}{h^3} dt_r + \frac{\Gamma_b}{4\pi} \frac{D_b}{h^3} dt_b \qquad (83)$$

where D_r' and D_3' are projections of D_r and D_3 on the X-Y plane.

Equation 83 produces a singularity if h is zero, which it may be if the point at which the velocity is being calculated is on the surface of the helical vortex sheet. This possibility is avoided by assuming that the vortex sheet originating on the quarter-chord is immediately swept down by the velocity normal to the tip path plane and that the instantaneous induced velocity may then be evaluated at the three-quarter chord line which lies above the vortex sheet.

For convenience, Cartesian and polar coordinates will be used simultaneously to define the geometry of the system. The point on the three-

quarter chord of the blade at which the induced velocity is to be calculated is $(x_1, y_1, 0)$, (r_1, ψ_1) and the location of the vortex element at the quarter chord of the wake blade is (x, y, z), (r, ξ). From Figure 17, the lengths which appear in Equation 83 may be evaluated:

$$h^2 = (x-x_1)^2 + (y-y_1)^2 + z^2 \tag{84}$$

$$D_r' = (x-x_1)\cos\xi - (y-y_1)\sin\xi \tag{85}$$

$$D_b = D_\xi' = -(x-x_1)\sin\xi - (y-y_1)\cos\xi \tag{86}$$

To evaluate x, y, and z, it is necessary to distinguish between blades if the rotor has more than one. Designate the blade at which the induced velocity is being computed as #1 and number counter clockwise to b. Then for the n th blade:

$$x = r\cos\xi + \mu R\left[\xi + \frac{(n-1)}{b}2\pi\right] \tag{87}$$

$$y = -r\sin\xi \tag{88}$$

Since the Z axis is taken as perpendicular to the tip path plane, the z distance for a point on the wake is equal to the velocity normal to the tip path plane multiplied by the time since that portion of the wake was generated. Thus:

$$z = \left[(\alpha + a_1)V - \bar{w}\right] \left[\frac{\psi_1 + \frac{(n-1)}{b} 2\pi + \xi}{\Omega}\right] \tag{89}$$

or $$z = (\lambda + \mu a_1) R \left[\psi_1 + \frac{(n-1)}{b} 2\pi + \xi\right] \tag{90}$$

Thus Equations 84-86 become:

$$h^2 = R^2 \left(\left\{ \frac{r}{R} \cos\xi + \mu \left[\xi + \frac{(n-1)}{b} 2\pi \right] - \frac{X_1}{R} \right\}^2 - \left\{ -\frac{r}{R} \sin\xi - \frac{Y_1}{R} \right\}^2 \right.$$

$$\left. + \left\{ (\lambda + \mu a_1) \left[\psi_1 + \frac{(n-1)}{b} 2\pi + \xi \right] \right\}^2 \right) \tag{91}$$

$$D_r' = R \left(\frac{r}{R} + \left\{ \mu \left[\xi + \frac{(n-1)}{b} 2\pi \right] - \frac{X_1}{R} \right\} \cos\xi + \frac{Y_1}{R} \sin\xi \right) \tag{92}$$

$$D_b = D_\xi' = R \left(-\left\{ \mu \left[\xi + \frac{(n-1)}{b} 2\pi \right] - \frac{X_1}{R} \right\} \sin\xi + \frac{Y_1}{R} \cos\xi \right) \tag{93}$$

The incremental distances, dt_r and dt_ξ, have the form:

$$dt_r = dt_b = R \, d\frac{r}{R} \sqrt{\left(\frac{\partial x}{\partial r}\right)^2 + \left(\frac{\partial y}{\partial r}\right)^2 + \left(\frac{\partial z}{\partial r}\right)^2} \tag{94}$$

and $$dt_\xi = d\xi \sqrt{\left(\frac{\partial x}{\partial \xi}\right)^2 + \left(\frac{\partial y}{\partial \xi}\right)^2 + \left(\frac{\partial z}{\partial \xi}\right)^2} \tag{95}$$

which give: $$dt_r = dt_b = R \, d\frac{r}{R} \tag{96}$$

and $$dt_3 = R\sqrt{\left(\frac{r}{R}\right)^2 - 2\mu\frac{r}{R}\sin\zeta + \mu^2 + (\lambda+\mu a_1)^2}\,d\zeta \qquad (97)$$

In Part I, expressions for circulation in normal flow and in reversed flow were derived. For the purposes of computing induced velocity, it will be assumed that the reversed flow region has little effect and that the expression for circulation in normal flow may be used over the entire rotor. For computing induced drag, the tip and root losses were accounted for by assuming that no lift was generated by those portions of the blade near the tip and root. Because of the extreme importance of the gradient of circulation near the blade tip in computing induced velocities, this simple approach to tip and root losses must be considered inadequate. To remedy this situation, the circulation distribution given by Equation 9 will be multiplied by a tip loss function, F, a function of r/R, which is unity over most of the blade but falls to zero at the root and tip. The method used to determine F will be described later. Correcting Equation 9 by multiplying by the tip loss factor and replacing ψ by $\psi_1 + \frac{n-1}{b}2\pi$ gives

$$\Gamma_b = \frac{\Omega R c a}{2}\left[\theta_0\frac{r}{R} + \theta_1\left(\frac{r}{R}\right)^2 + \lambda + \left(\theta_0\mu + \frac{r}{R}\mu\theta_1 - \frac{r}{R}a_1\right)\sin\left(\psi_1 + \frac{n-1}{b}2\pi\right)\right.$$

$$+ \left(\frac{r}{R}b_1 - \mu a_0\right)\cos\left(\psi_1 + \frac{n-1}{b}2\pi\right) + \mu a_1\cos^2\left(\psi_1 + \frac{n-1}{b}2\pi\right)$$

$$\left. + \mu b_1\sin\left(\psi_1 + \frac{n-1}{b}2\pi\right)\cos\left(\psi_1 + \frac{n-1}{b}2\pi\right)\right] F \qquad (98)$$

Differentiating Equation 9 with Ψ replaced by $-\xi$ gives:

$$\frac{\partial \Gamma}{\partial \frac{r}{R}} = \frac{\Omega R c a}{2} \left\{ \left[\theta_0 + 2\theta_1 \frac{r}{R} - (\mu\theta_1 - a_1)\sin\xi + b_1 \cos\xi \right] F \right.$$

$$+ \left[\theta_0 \frac{r}{R} + \theta_1 \left(\frac{r}{R}\right)^2 + \lambda - \left(\theta_0 \mu + \frac{r}{R}\mu\theta_1 - \frac{r}{R} a_1\right)\sin\xi \right.$$

$$\left. \left. + \left(\frac{r}{R} b_1 - \mu a_0\right)\cos\xi + \mu a_1 \cos^2\xi - \mu b_1 \sin\xi\cos\xi \right] F' \right\} \qquad (99)$$

$$\frac{\partial \Gamma}{\partial \xi} = \frac{\Omega R c a}{2} \left[-\left(\theta_0 \mu + \frac{r}{R}\mu\theta_1 - \frac{r}{R} a_1\right)\cos\xi - \left(\frac{r}{R} b_1 - \mu a_0\right)\sin\xi \right.$$

$$\left. - 2\mu a_1 \cos\xi \sin\xi - \mu b_1 (2\cos^2\xi - 1) \right] F \qquad (100)$$

Except for F and F', we now have all of the terms required by equation 82 in Equations 91-93, and 96-100. The total induced velocity, w, is found from the double integration on ξ and r/R and the summation over the several blades: (next page)

$$\frac{8\pi}{\lambda c a}\; w = \sum_{n=1}^{b} \int_{\frac{r_0}{R}}^{1} d\frac{r}{R} \int_{-\left[\psi_1 + \frac{n-1}{b} 2\pi\right]}^{\infty} \frac{\left(\left\{\left[A_1 + A_2 \frac{r}{R}\right] F + \left[A_3 + A_4 \frac{r}{R} + A_1 \left(\frac{r}{R}\right)^2\right] F'\right\}\left\{B_1 + \frac{r}{R} + A_5 \xi\right\} \sqrt{A_6 + A_7 \frac{r}{R} + \left(\frac{r}{R}\right)^2} + \left\{\left[A_8 + A_9 \frac{r}{R}\right]\left[B_2 + A_{10} \xi\right] F\right\}\right) d\xi}{\left(\left\{A_{11} \frac{r}{R} + B_3 + \mu \xi\right\}^2 + \left\{A_{12} \frac{r}{R} + B_4\right\}^2 + \left\{(\lambda + \mu a_1)\left[\psi_1 + \frac{n-1}{b} 2\pi + \xi\right]\right\}^2\right)^{\frac{3}{2}}}$$

$$+ \sum_{n=2}^{b} \int_{\frac{r_0}{R}}^{1} \frac{\left[C_3 + C_1 \frac{r}{R} + A_1 \left(\frac{r}{R}\right)^2\right]\left[D_2 - C_{10}\left(\psi_1 + \frac{n-1}{b} 2\pi\right)\right] F \; d\frac{r}{R}}{\left(\left\{C_{11} \frac{r}{R} + B_3 - \mu\left[\psi_1 + \frac{n-1}{b} 2\pi\right]\right\}^2 \left\{C_{12} \frac{r}{R} + B_4\right\}^2\right)^{\frac{3}{2}}} \qquad (101)$$

where $A_1 = -(\mu\theta_1 - a_1)\sin\xi + b_1\cos\xi + \theta_0$ (102)

$A_2 = 2\theta_1$ (103)

$A_3 = \mu(-\theta_0\sin\xi - a_0\cos\xi - b_1\sin\xi\cos\xi + a_1\cos^2\xi) + \lambda$ (104)

$A_4 = \theta_1$ (105)

$A_5 = \mu\cos\xi$ (106)

$A_6 = \mu^2 + (\lambda + \mu a_1)^2$ (107)

$A_7 = -2\mu\sin\xi$ (108)

$A_8 = \mu\left[-\theta_0\cos\xi - 2a_1\cos\xi\sin\xi - b_1(2\cos^2\xi - 1) + a_0\sin\xi\right]$ (109)

$A_9 = -b_1\sin\xi + (a_1 - \mu\theta_1)\cos\xi$ (110)

$A_{10} = -\mu\sin\xi$ (111)

$A_{11} = \cos\xi$ (112)

$A_{12} = -\sin\xi$ (113)

$B_1 = -\frac{x_1}{R}\cos\xi + \frac{y_1}{R}\sin\xi$ (114)

$$B_2 = \frac{X_1}{R} \sin \xi \tag{115}$$

$$B_3 = -\frac{X_1}{R} \tag{116}$$

$$B_4 = -\frac{Y_1}{R} \tag{117}$$

$$\frac{X_1}{R} = \frac{r_1}{R} \cos \psi_1 - \mu \psi_1 + \frac{c}{2R} \sin \psi_1 \tag{118}$$

$$\frac{Y_1}{R} = \frac{r_1}{R} \sin \psi_1 - \frac{c}{2R} \cos \psi_1 \tag{119}$$

$$C_1 = (\mu \theta_1 - a_1) \sin\left[\psi_1 + \frac{(n-1)}{b} 2\pi\right] + b_1 \cos\left[\psi_1 + \frac{(n-1)}{b} 2\pi\right] + \theta_0 \tag{120}$$

$$C_3 \quad \mu \Big\{ -\theta_0 \sin\left[\psi_1 + \frac{(n-1)}{b} 2\pi\right] - a_0 \cos\left[\psi_1 + \frac{(n-1)}{b} 2\pi\right]$$

$$- b_1 \sin\left[\psi_1 + \frac{(n-1)}{b} 2\pi\right] \cos\left[\psi_1 + \frac{(n-1)}{b} 2\pi\right]$$

$$+ a_1 \cos^2\left[\psi_1 + \frac{(n-1)}{b} 2\pi\right] \Big\} + \lambda \tag{121}$$

$$C_{11} = \cos\left[\psi_1 + \frac{(n-1)}{b} 2\pi\right] \tag{122}$$

$$C_{12} = -\sin\left[\psi_1 + \frac{(n-1)}{b} 2\pi\right] \tag{123}$$

$$D_2 = -\frac{X_1}{R} \sin\left[\psi_1 + \frac{(n-1)}{b} 2\pi\right] \tag{124}$$

3. Tip Loss Function:

In the determination of the induced velocity, w, a very important factor is the value of the radial component of the circulation gradient, $\frac{\partial \Gamma}{\partial \bar{r}}$ near the root and tip. This quantity, in turn, is primarily a function of the assumed tip loss function which specifies the manner in which the circulation goes to zero at the root and tip. Two possible approaches for determining the tip loss function present themselves. In the first, the tip loss function for a hovering rotor (and by assumption, for a rotor in forward flight) may be determined theoretically using Goldstein's Modified Vortex Method as outlined by Nikolsky in Section 2.3 of Reference 7. Since the Goldstein Method is strictly applicable only to a propeller with a certain combination of taper and twist, it is not certain that it will give good results for an untapered rotor blade with arbitrary twist. For this reason, the second approach, a semi-empirical method based on measured lift distributions is recommended. Using this method, a tip loss factor based on a measured lift distribution given by Fallabella and Meyer in Reference 8 has been determined. In detail, the steps which have been taken are:

1. The lift distribution for a single-bladed rotor at $\psi = 0^\circ$ was taken from Figure 25 of Reference 8. (The tip loss function for $\psi = 0^\circ$ was assumed to apply to all values of ψ.)
2. The measured lift distribution was divided by r/R to give $(\rho \Omega R)\Gamma$ and the result was plotted on Figure 18a.
3. Equation 9 was written for $\psi = 0^\circ$, $\theta_1 = 0$ with the value of θ_0, b_1, μ, a_0, and a_1 from Table I of Reference 8 to give:

$$\Gamma = \frac{\Omega R c a}{2} \left[.1797 \frac{r}{R} + .0298 + \lambda \right] \qquad (125)$$

4. The experimental value of λ at $\psi = 0^{\circ}$ as a function of radius was taken from Figure 27 of Reference 8 and plotted on Figure 18b.

5. To avoid a double accounting for tip loss, the curve for λ on Figure 18b was modified outboard of r/R = .65 to obtain an estimated value of λ without tip effect.

6. Using the modified value of λ, the bracketed term of Equation 125 was evaluated to give $\left(\frac{2}{\Omega R c a}\right)\Gamma$ as a function of r/R.

7. The theoretical distribution of $\left(\frac{2}{\Omega R c a}\right)\Gamma$ from step 6 was made to match the measured distribution of $(\rho \Omega R)\Gamma$ from step 2 at r/R = .65 by multiplying by a constant, which in this case was 6.06.

8. The distribution of $6.06\left(\frac{2}{\Omega R c a}\right)\Gamma$ was then plotted on Figure 18a to provide a comparison between the theoretical and experimental circulation distributions.

9. Since no experimental points were available outboard of r/R = .96, the experimental circulation at the extreme tip was assumed to have the form:

$$\Gamma_{TIP} = k\sqrt{1-\frac{r}{R}} \tag{126}$$

where k is a constant which makes r/R = .96 a match point and in this case is 1.435.

10. The tip loss function, F, was obtained by dividing the experimental circulation distribution by the theoretical distribution, and the result was plotted on Figure 19.

11. At the root, $r = r_o$, a mirror image of the tip loss function was plotted to represent root loss.

The experimental lift distribution used to determine the tip loss function in this example was for a rotor with a blade aspect ratio of 10. Since experimental lift distributions for other aspect ratios are not readily available, it is suggested that the tip loss function for aspect ratio of 10 may be generally used if the tip loss is assumed to start 3.5 chord lengths from the tip and the horizontal scale modified accordingly.

At this time the sensitivity of the calculation of induced velocity to the exact shape of the tip loss function is not known. It is hoped that calculations now underway will provide an answer to this question.

D. NUMERICAL EXAMPLE

The numerical integration of Equation 101 has been programmed for the Datatron Digital Computer on the campus of the California Institute of Technology. The integral is evaluated at 15 points along the blade and for every 20° of ζ . The flight and physical parameters for the test of the one-bladed rotor presented in Reference 8 have been used in an attempt to check the theory against experiment, but unfortunately, recently discovered coding errors have made it necessary to throw out all numerical results obtained up to the time of this writing. The project is to be continued, however, and the results will be reported when obtained.

CONCLUSIONS

A method for computing the vertical component of the instantaneous induced velocity at a rotor blade due to the wake of a finite bladed rotor has been developed. The method requires numerical integration such as is most conveniently done with a high speed digital computer. A computing program has been written for the Datatron Computer, but at this time no numerical results can be reported.

REFERENCES

1. Von Mises: Theory of Flight. McGraw-Hill Book Co., New York, 1945

2. Bailey: A Simplified Method of Determining the Characteristics of a Lifting Rotor in Forward Flight. NACA TR 716, 1941

3. Whittaker and Robinson: The Calculus of Observations. Blackie and Son Ltd., London, 1924

4. Gessow and Tapscott: Charts for Estimating Performance of High Performance Helicopters. NACA TN 3323, 1955

5. Perkins and Hage: Airplane Performance, Stability, and Control. John Wiley and Sons, New York, 1949

6. Heyson: Analysis and Comparison with Theory of Flow-Field Measurements Near a Lifting Rotor in the Langley Full-Scale Tunnel. NACA TN 3691, 1956

7. Nikolsky: Helicopter Analysis. John Wiley and Sons, New York, 1951

8. Falabella and Meyer: Determination of Inflow Distributions from Experimental Aerodynamic Loading and Blade-Motion Data on a Model Helicopter Rotor in Hovering and Forward Flight. NACA TN 3492, 1955

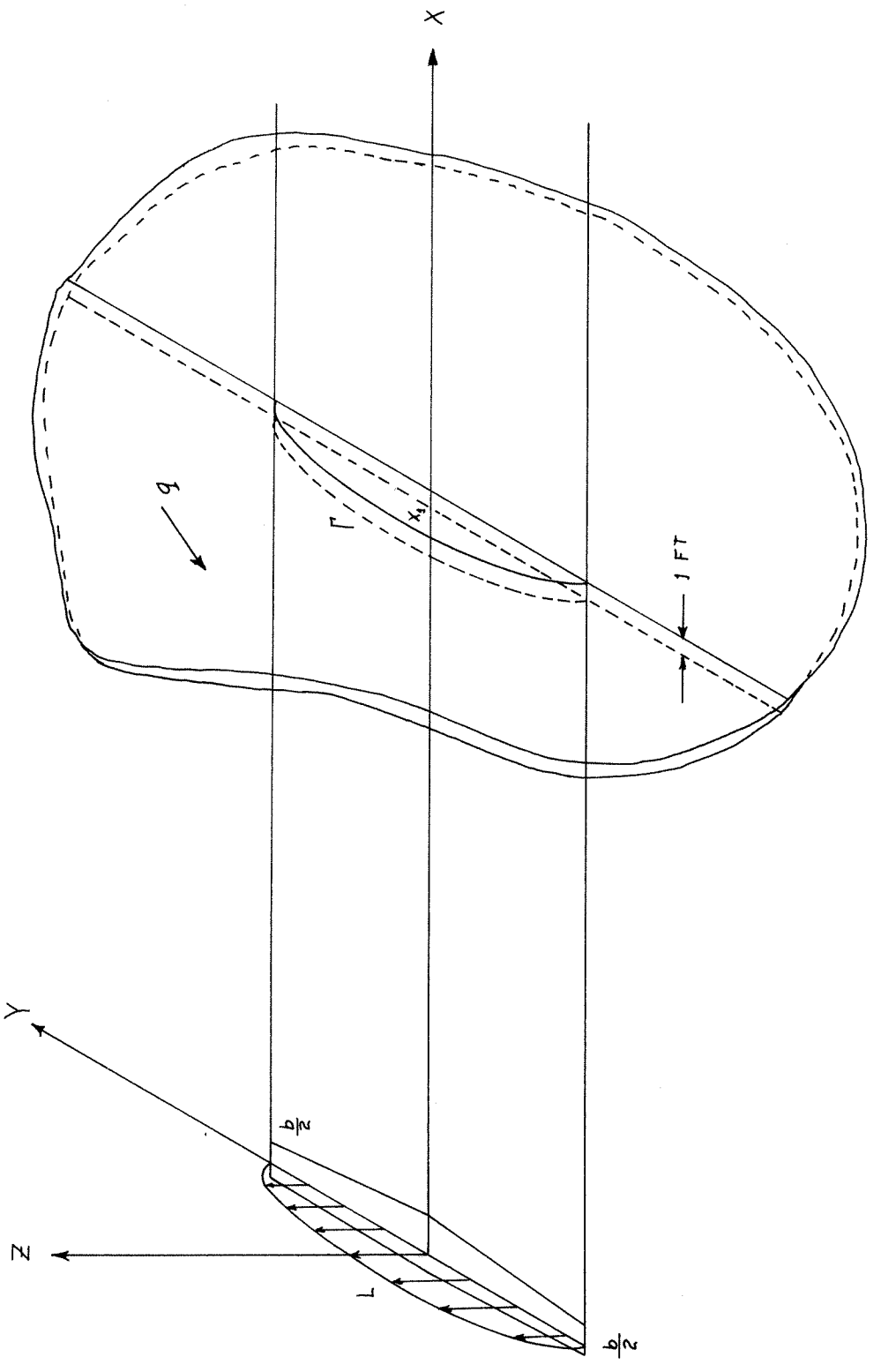

Figure 1.- Wake of Wing

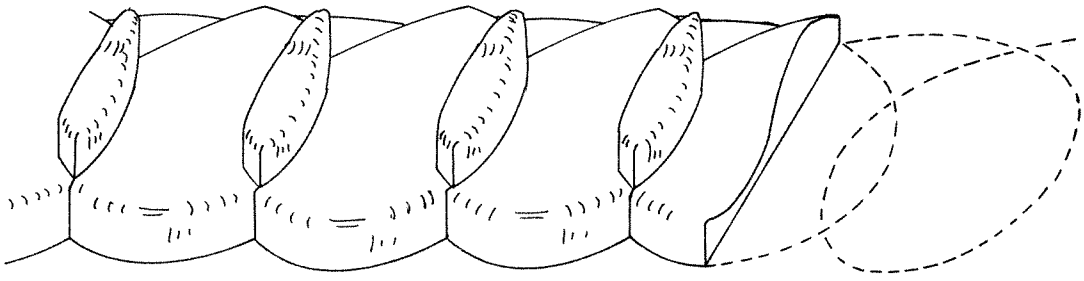

Figure 2a.- Distribution of Circulation in Wake of One-Bladed Rotor

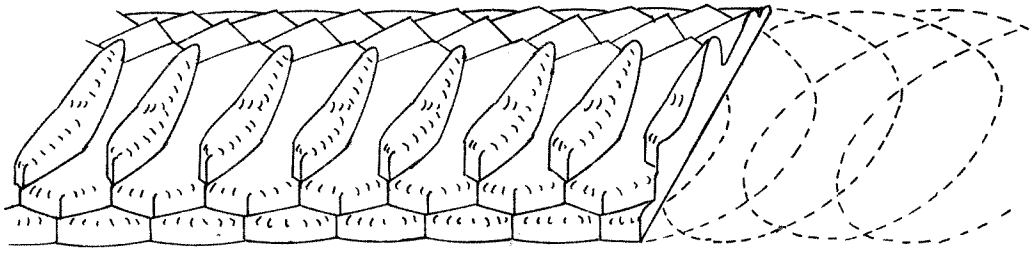

Figure 2b.- Distribution of Circulation in Wake of Two-Bladed Rotor

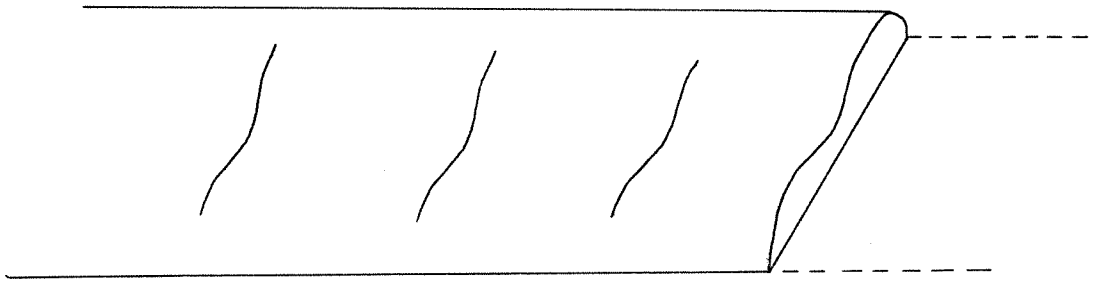

Figure 2c.- Distribution of Circulation in Wake of Infinite-Bladed Rotor

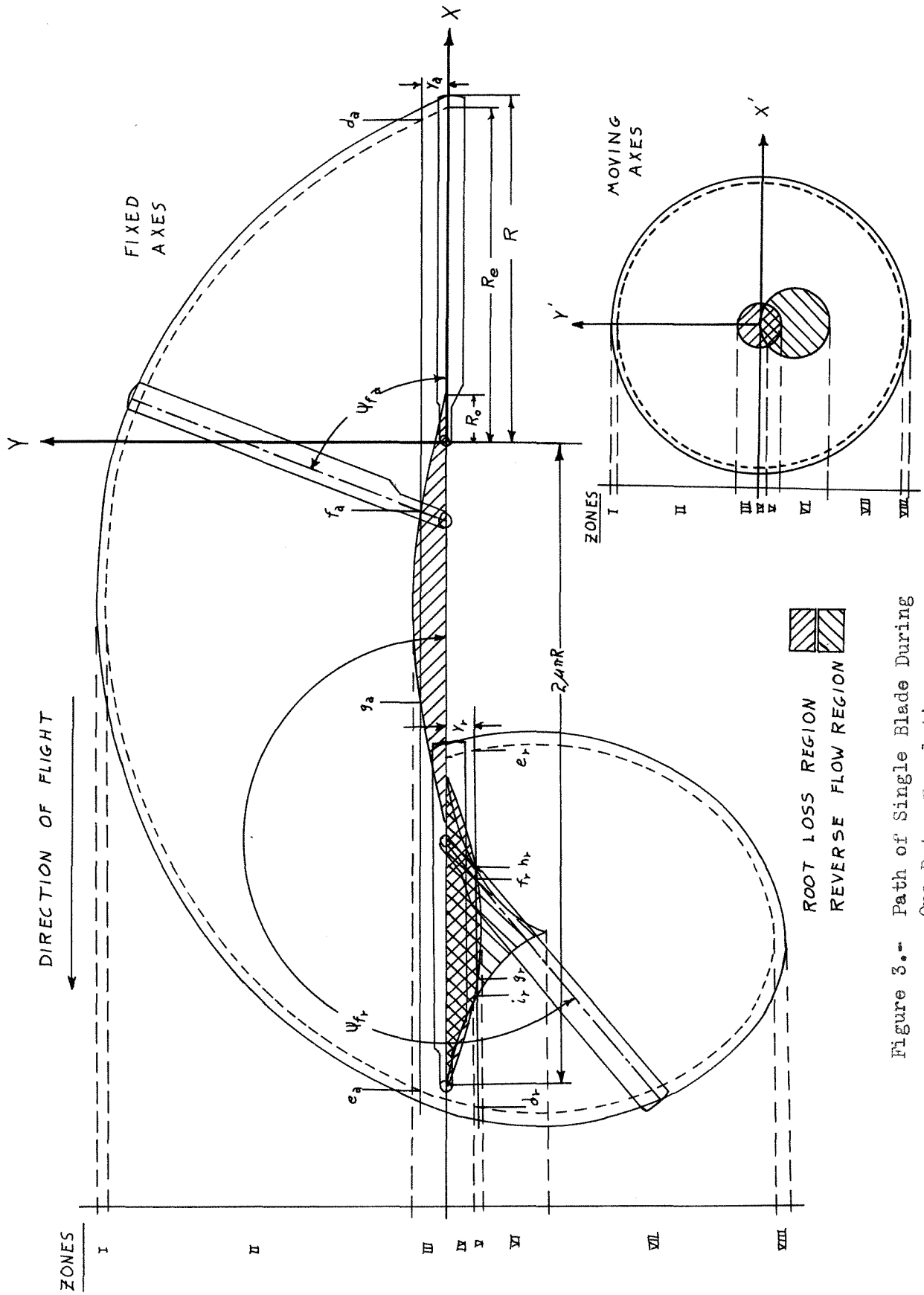

Figure 3.- Path of Single Blade During One Rotor Revolution

Figure 4.- Induced Drag Ratio, $1+\delta$, for 0° Twist

$$D_i = (1+\delta)\frac{T^2}{2\rho A V^2}$$

$\frac{R_e}{R} = .97$

$\frac{R_o}{R} = .10$

$-\alpha_s = -8°$

$+ \quad \lambda = 0$

$\times \quad \lambda = -.05$

$\Delta \quad \lambda = -.10$

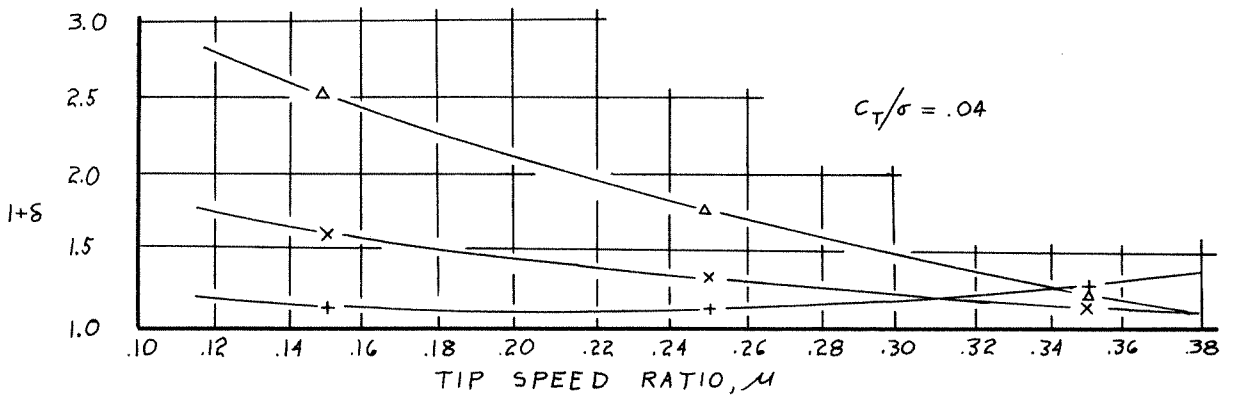

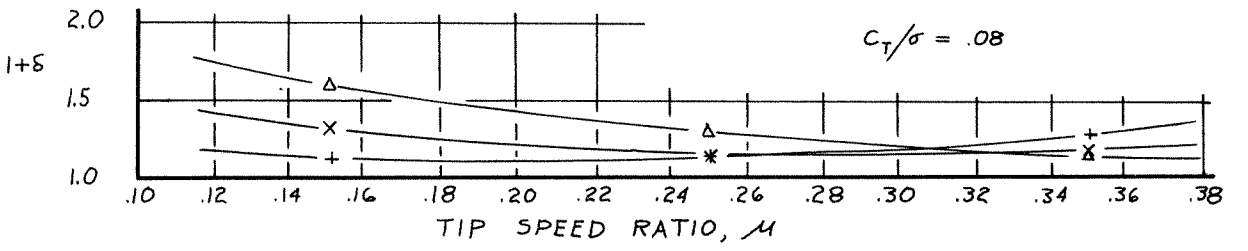

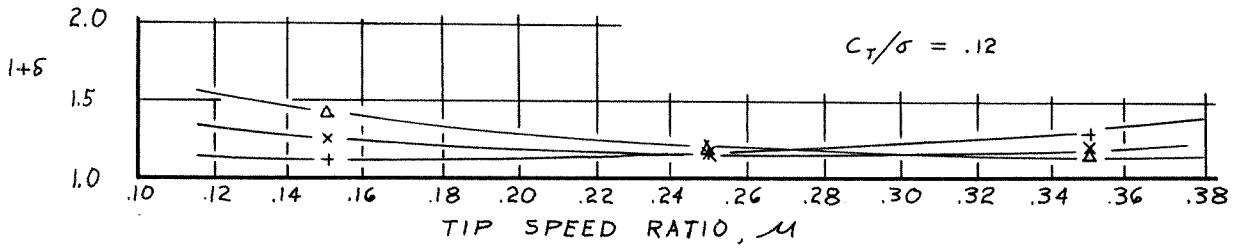

Figure 5.- Induced Drag Ratio, $1+\delta$, for -8° Twist

$$D_i = (1+\delta)\frac{T}{2\rho A V^2}$$

$\frac{R_e}{R} = .97$

$\frac{R_o}{R} = .10$

$-\alpha_s = -8^\circ$

+ $\lambda = 0$

× $\lambda = -.05$

△ $\lambda = -.10$

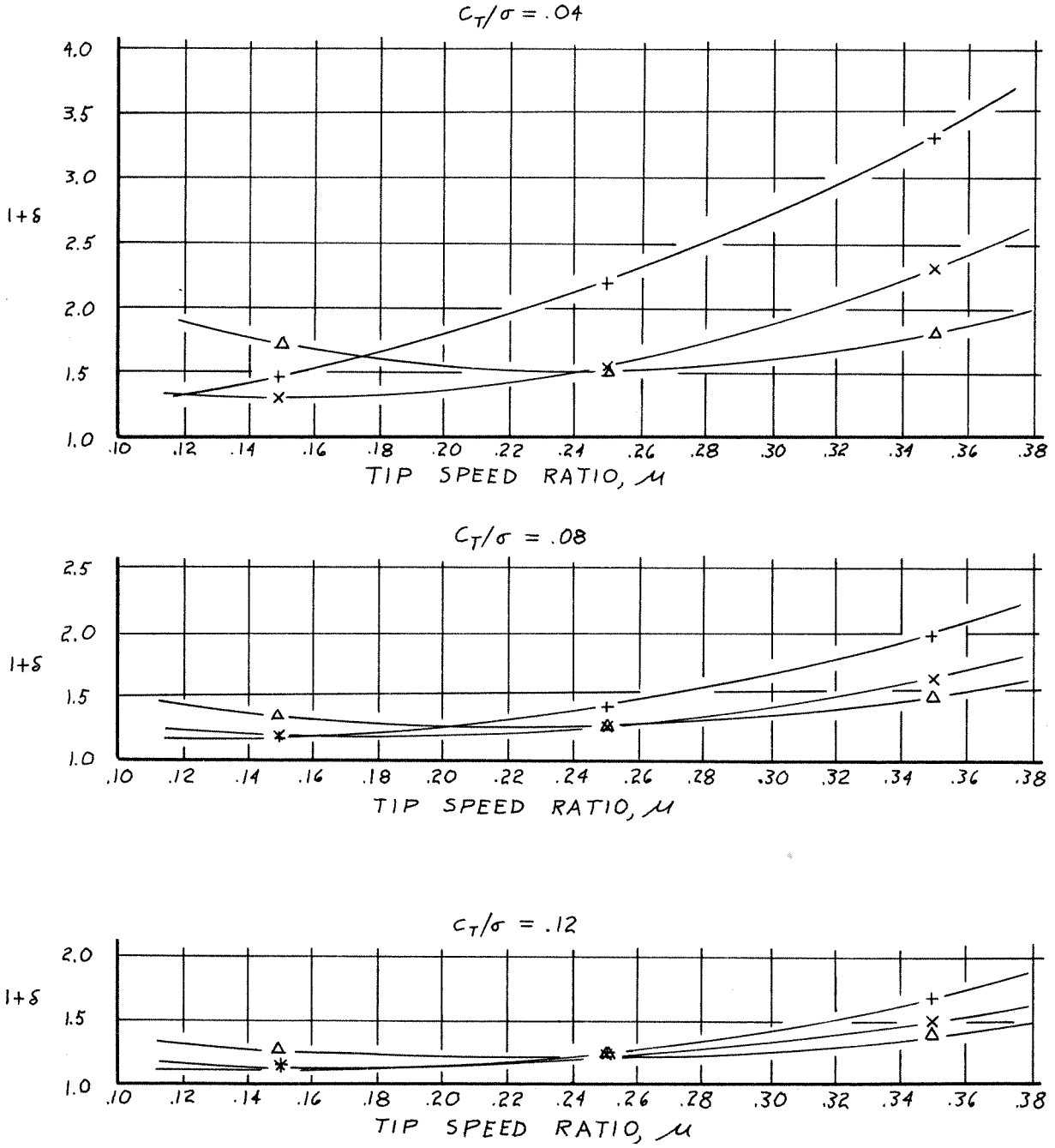

Figure 6.- Induced Drag Ratio, $1+\delta$, for -16° Twist

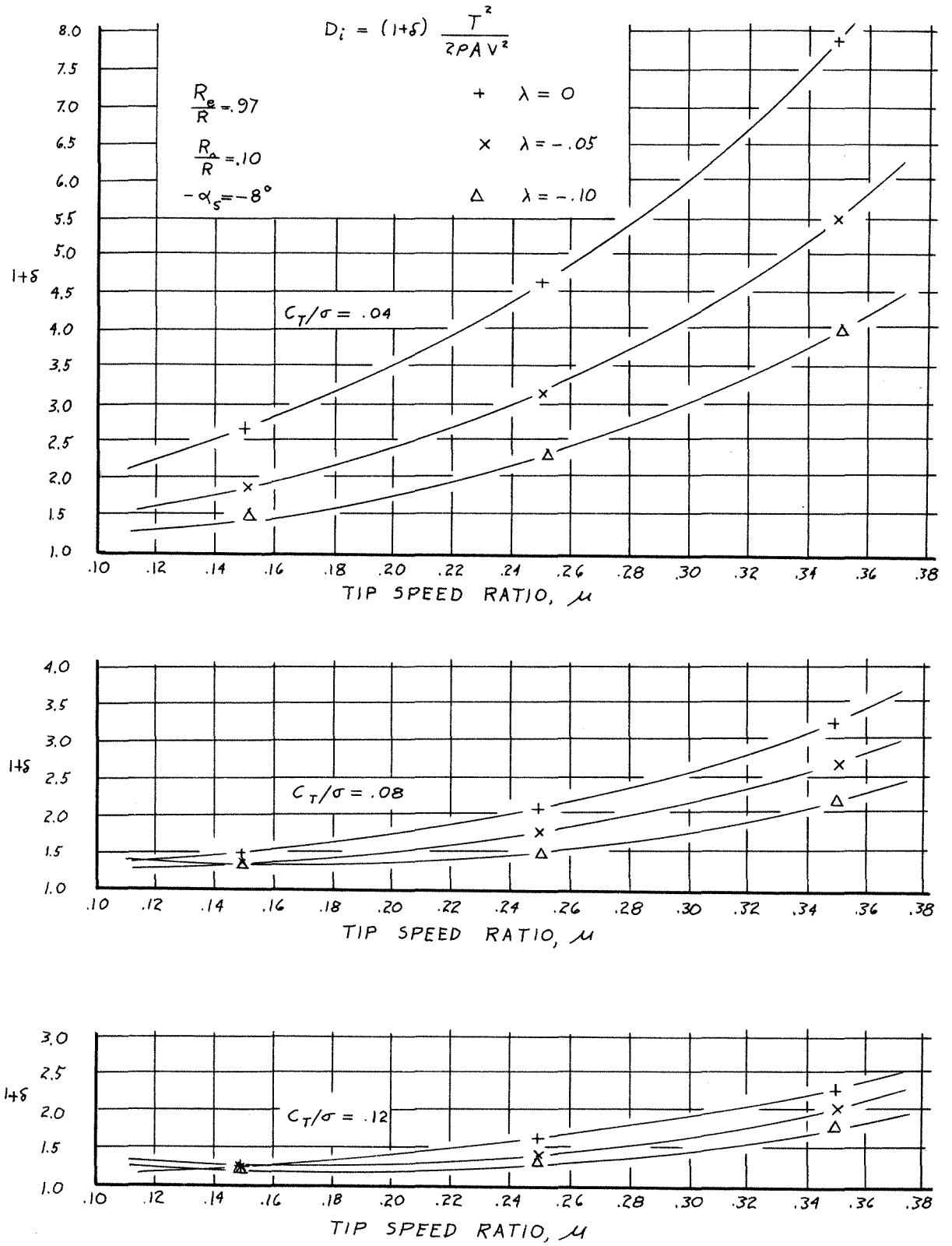

Figure 7.- Effect of Twist, θ_1, on

Distribution of Circulation Coefficient, C_Γ

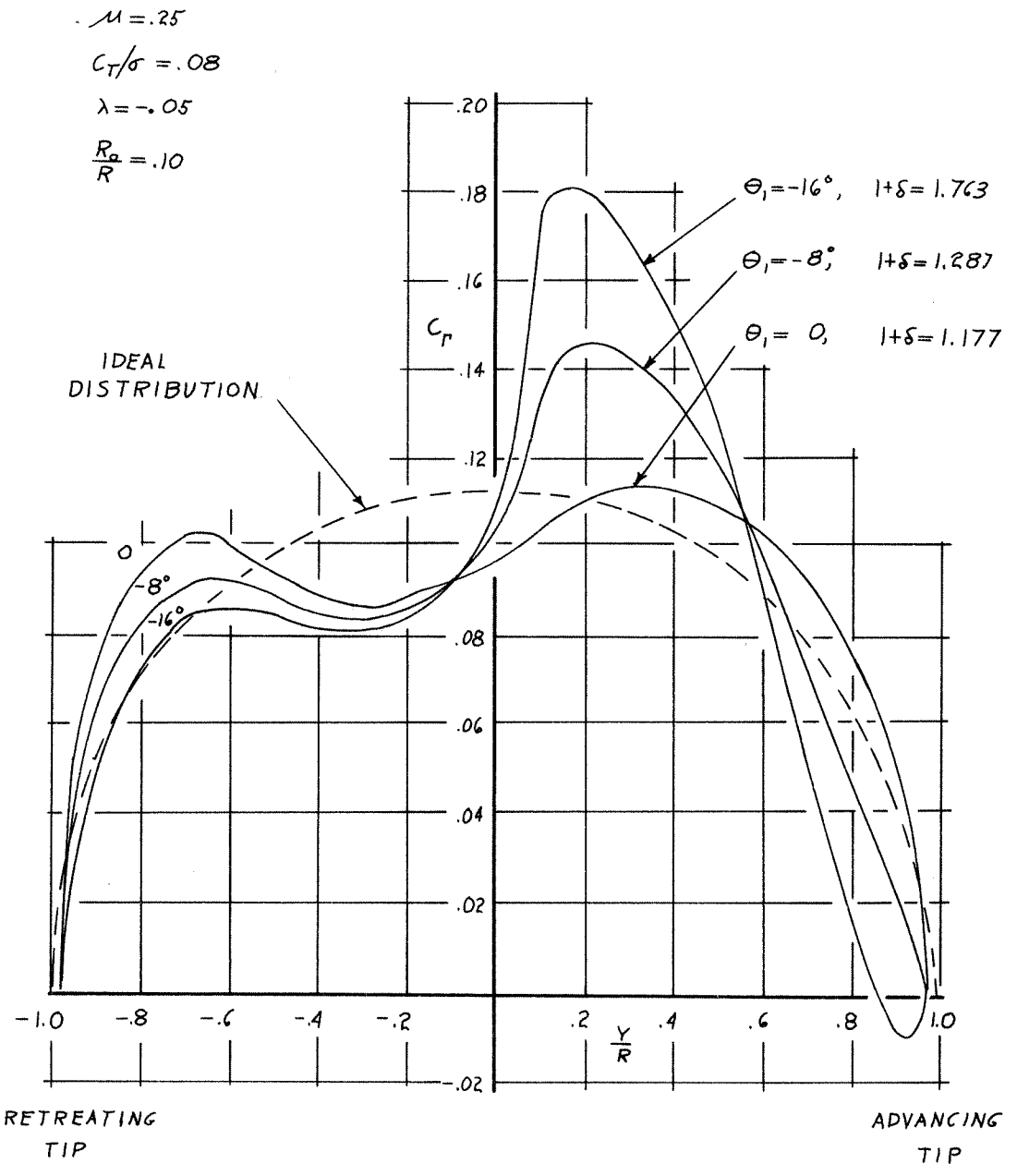

Figure 8.- Effect of Tip Speed Ratio, μ, on Distribution of Circulation Coefficient, C_r

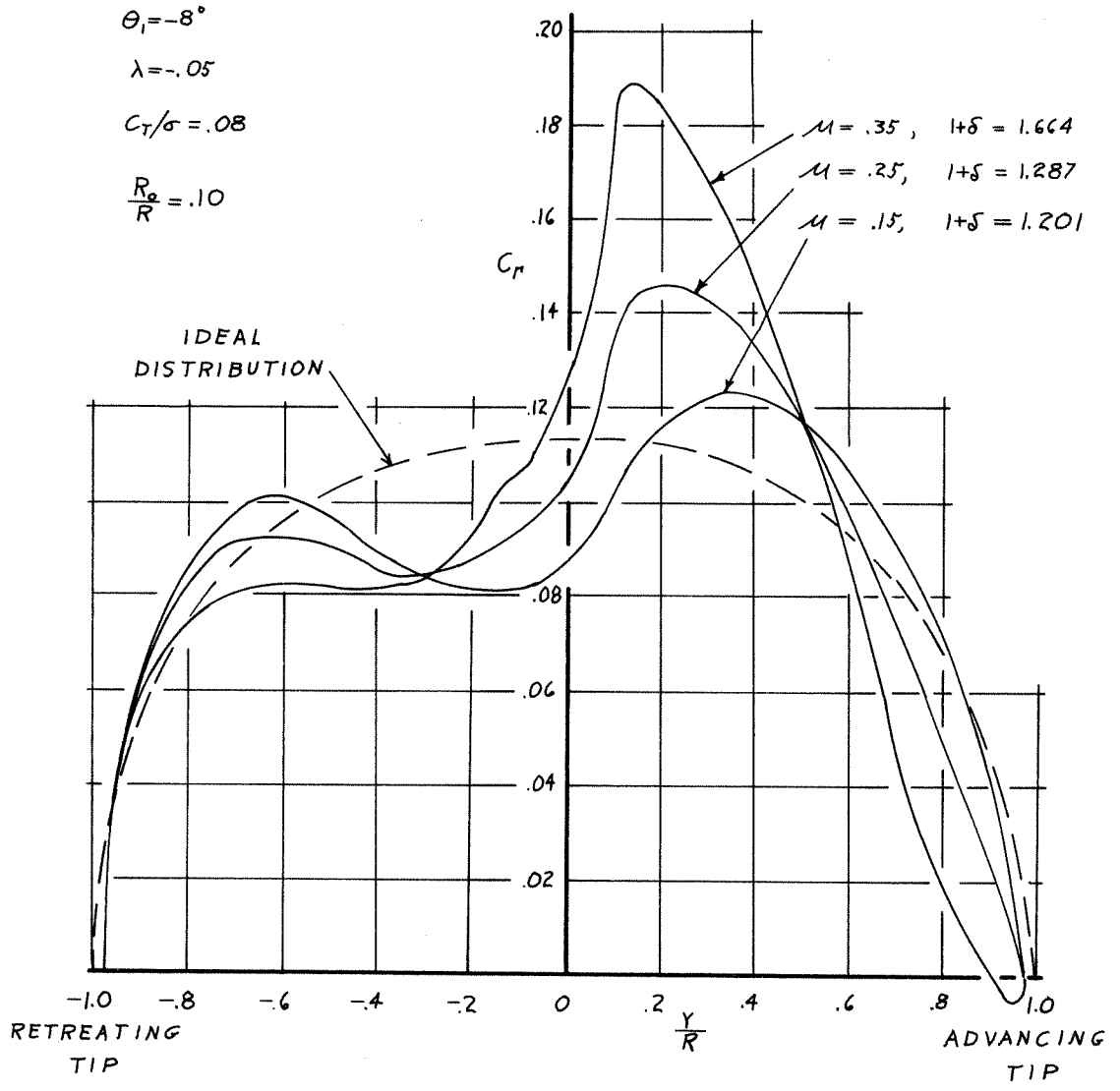

Figure 9.- Effect of Thrust/Solidity Ratio, C_T/σ, on Distribution of Circulation Coefficient, C_Γ

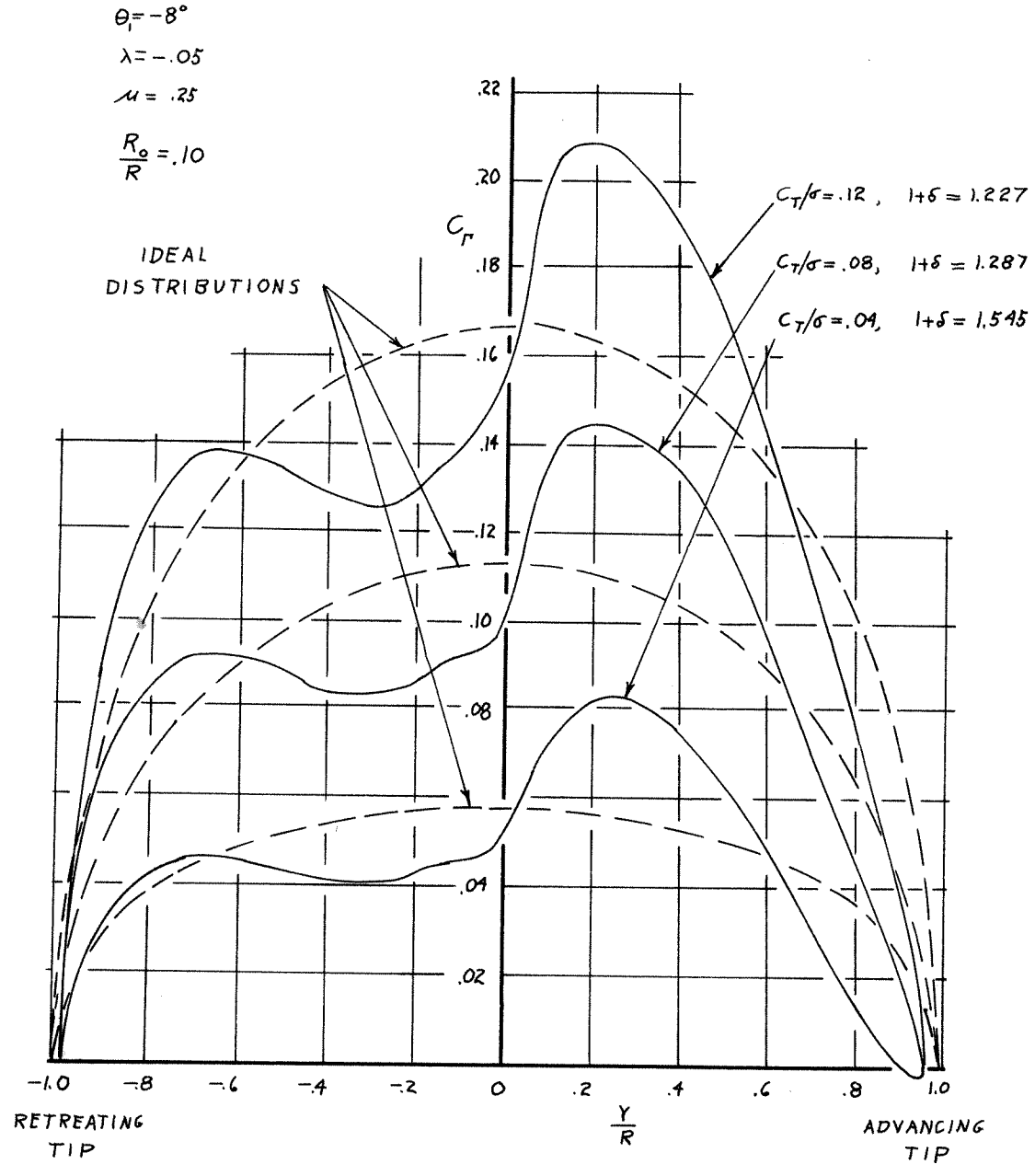

Figure 10.- Effect of Inflow Ratio, λ, on Distribution of Circulation Coefficient, C_Γ

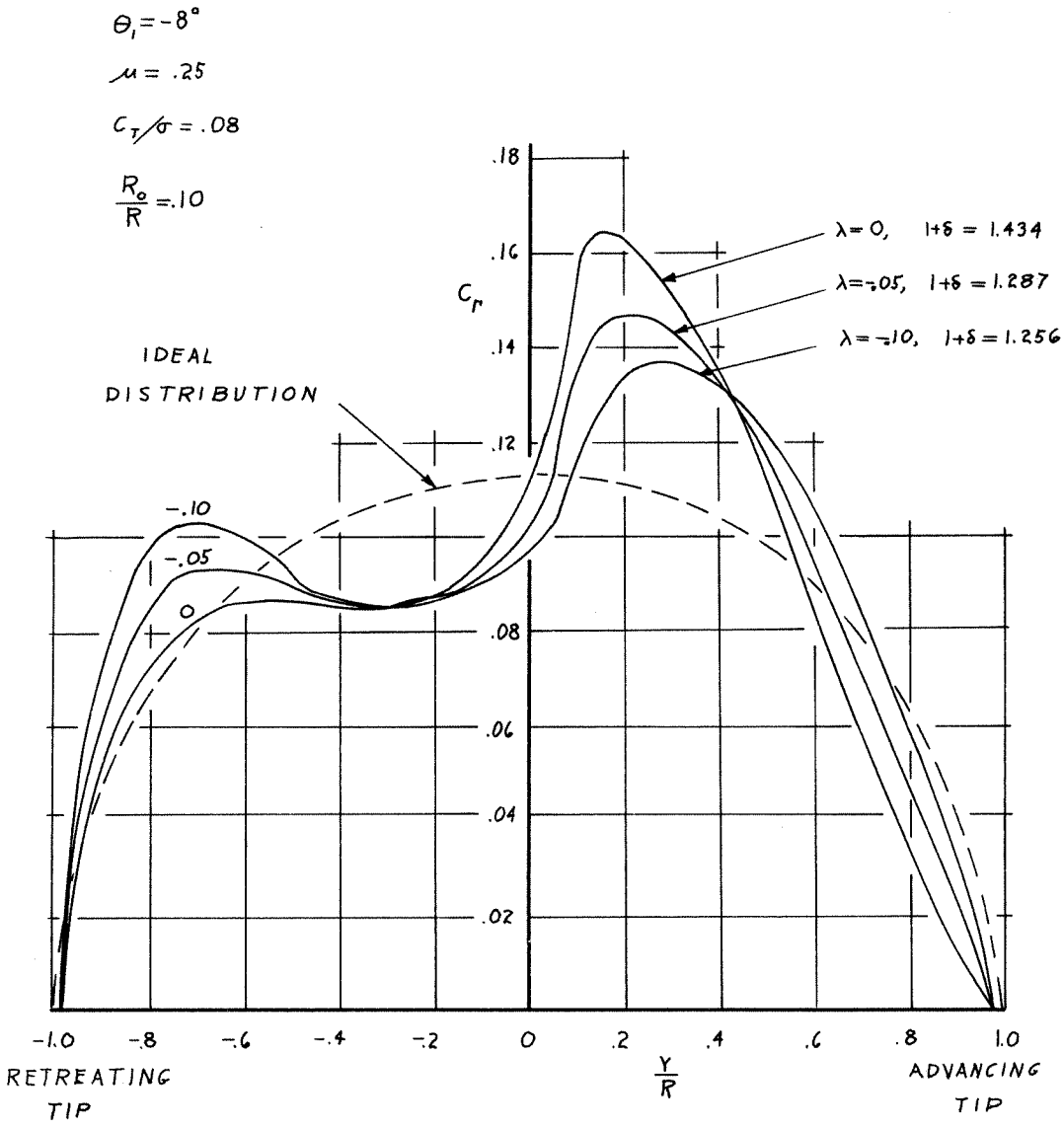

Figure 11.- Circulation Coefficient Distributions for Maximum and Minimum Values of $(1+\delta)$ Obtained During Computing Program

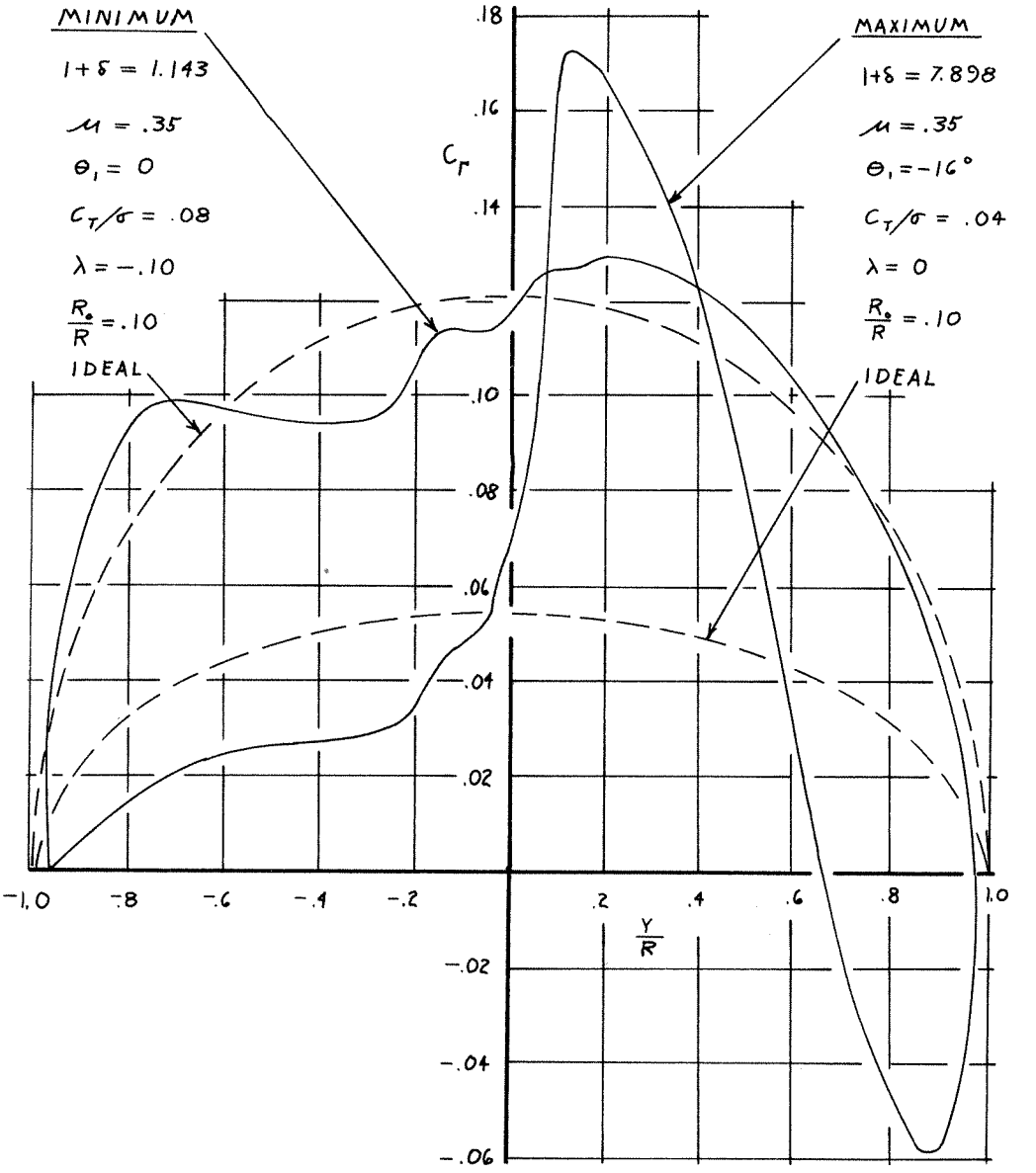

Figure 12.- Convergence of Induced Drag Series

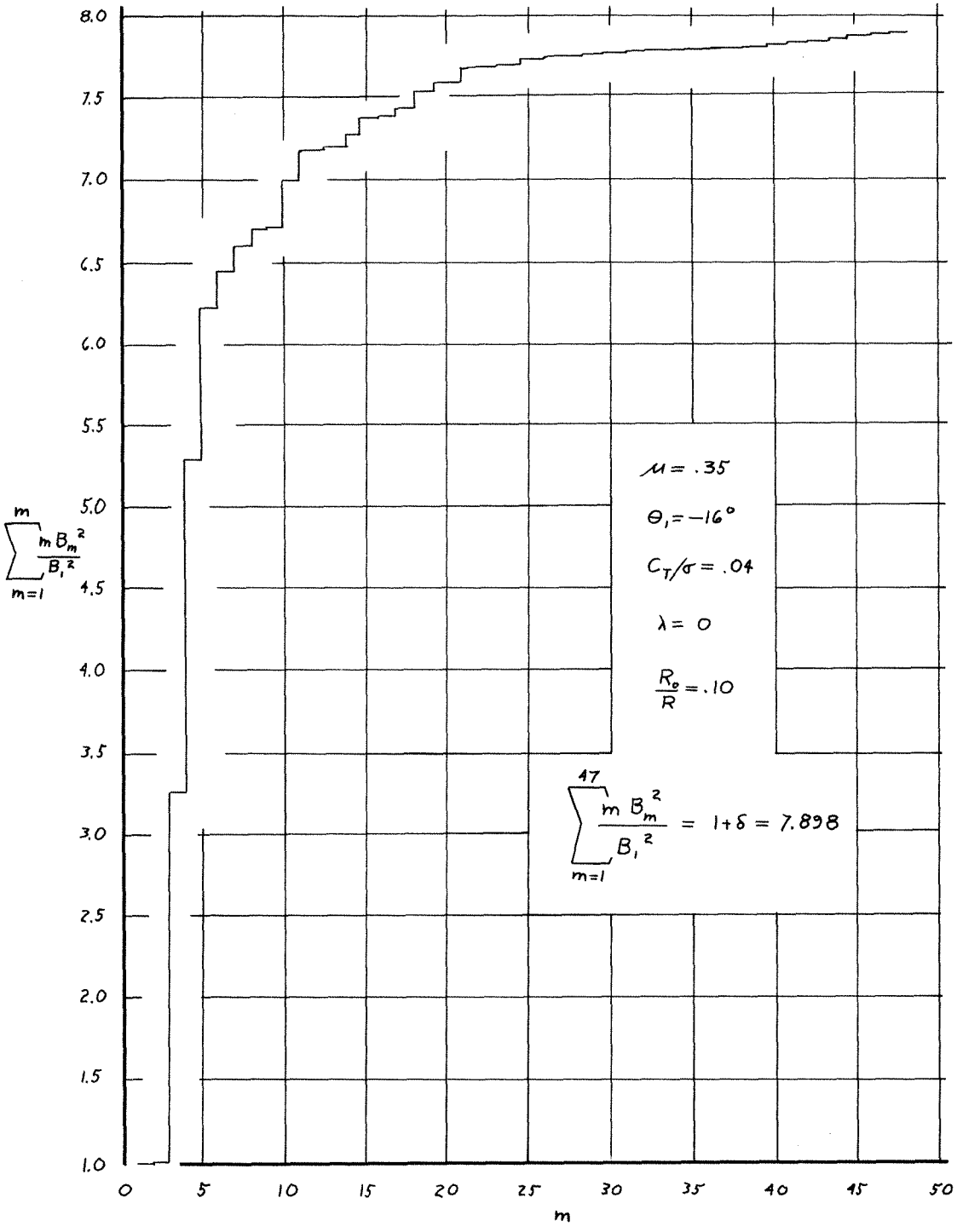

Figure 13.- Effect of Root Loss on Distribution of Circulation Coefficient, C_Γ

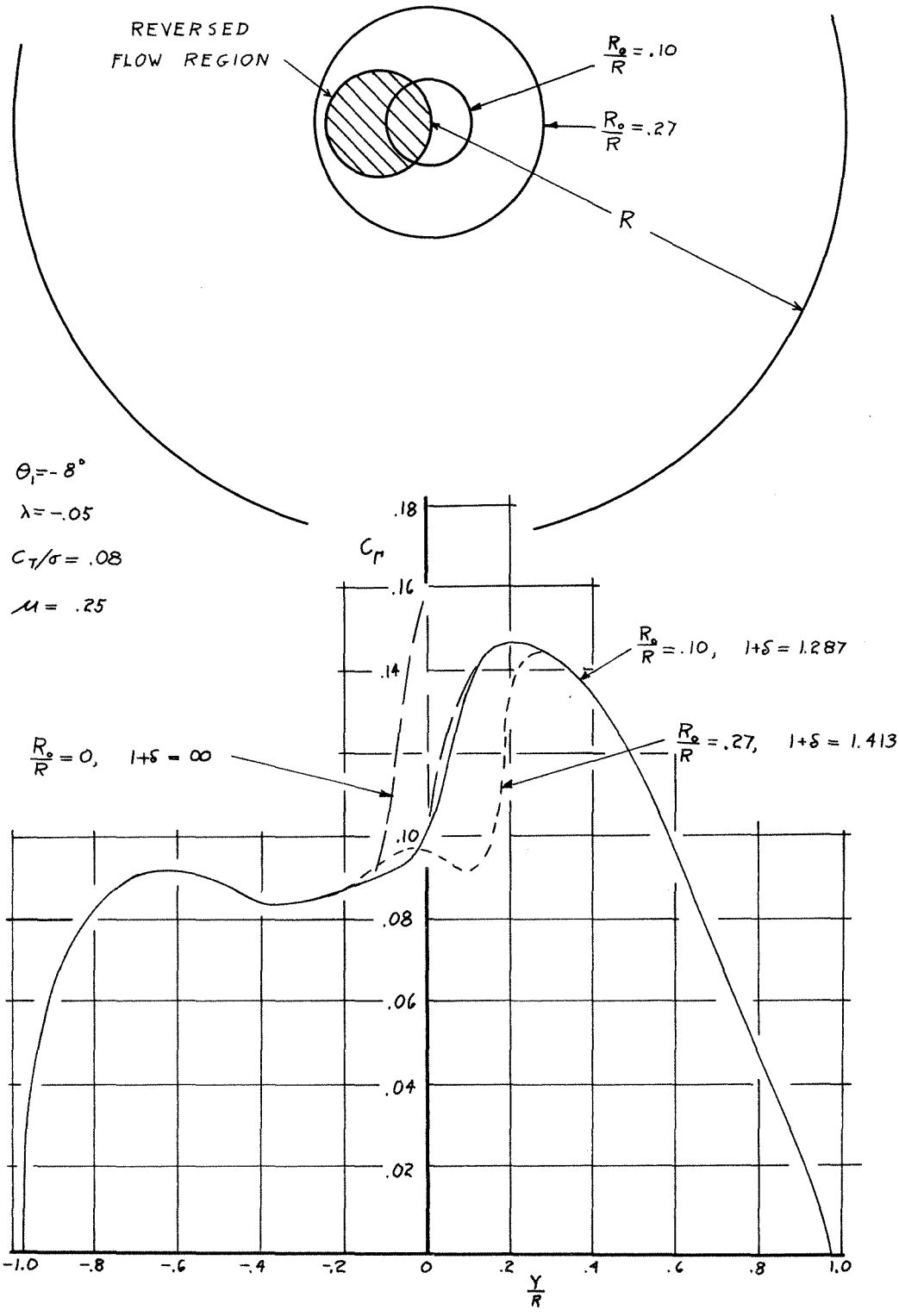

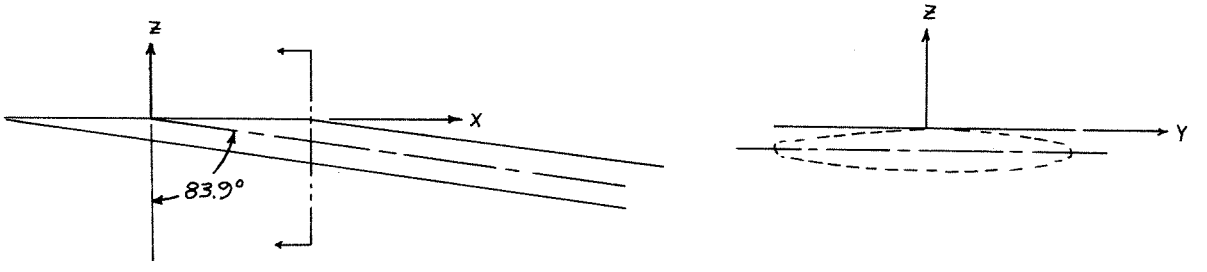

$R = 7.5$ FT

$\sigma = .0543$

$b = 2$

$\theta_1 = 0$

$\Omega = 60$ RAD/SEC

$\mu = .232$

$\lambda = -.046$

$C_T/\sigma = .059$

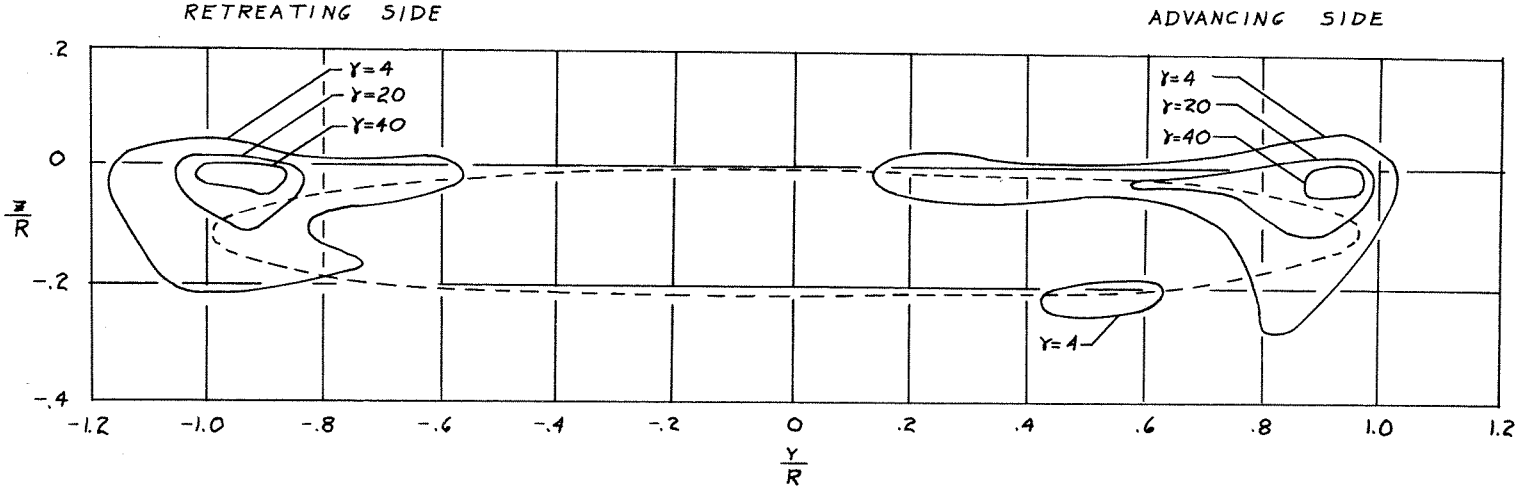

Figure 14.- Measured Distribution of Vorticity at x/R = 1.07

(Taken from Fig. 52, NACA TN 3691)

Figure 15.- Experimental and Calculated Distribution of Circulation, Γ

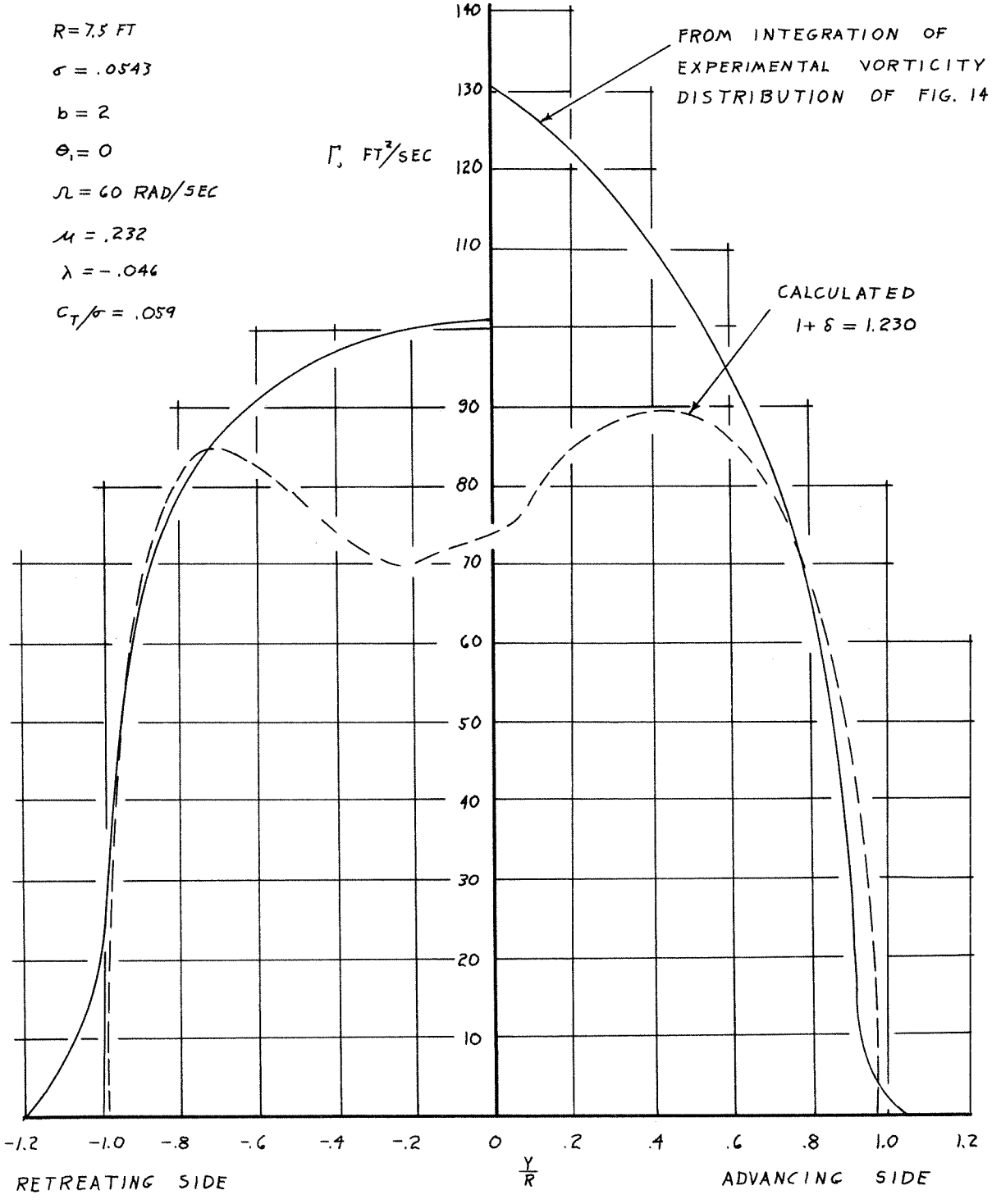

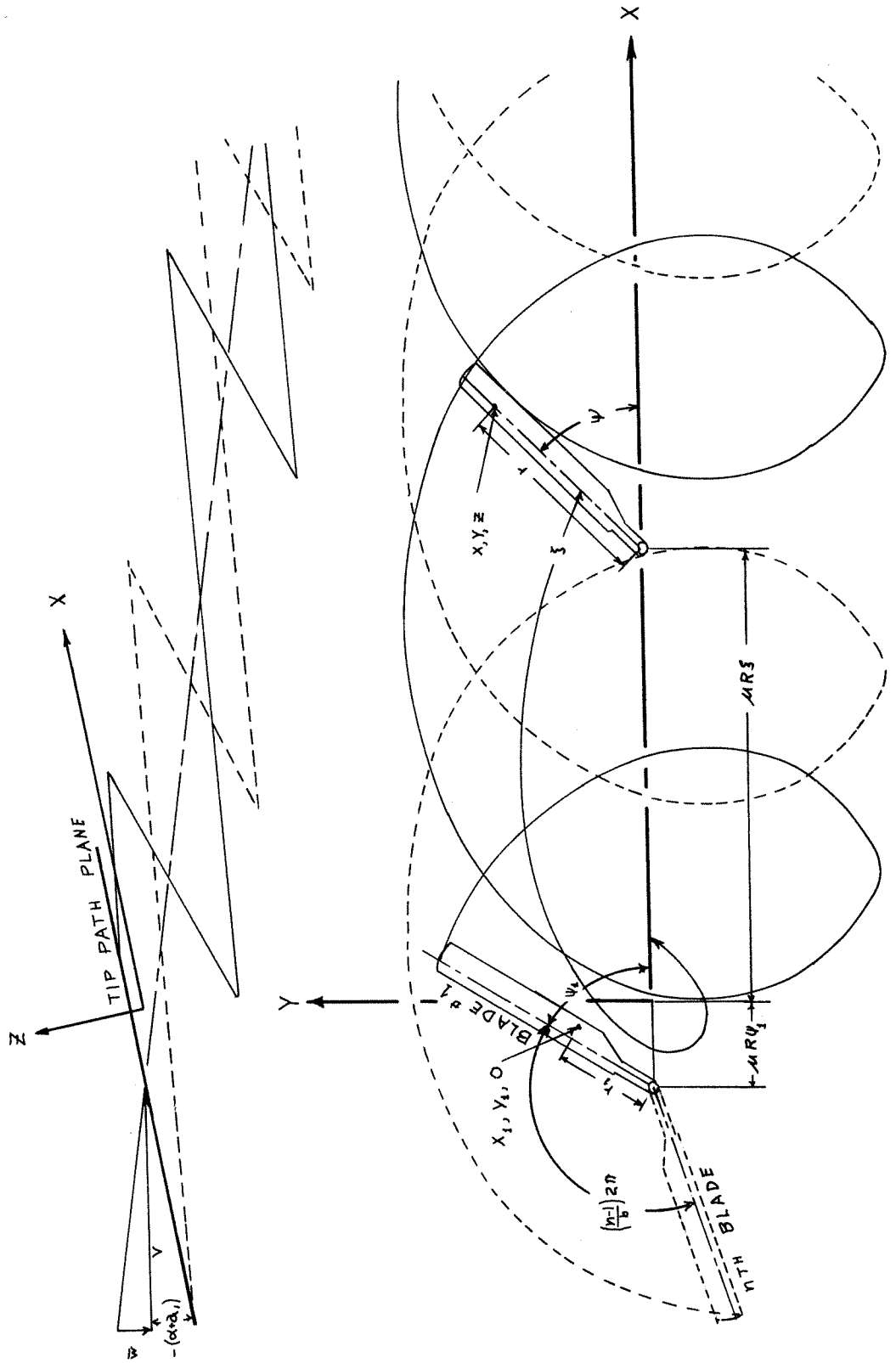

Figure 16.- Wake of Finite-Bladed Rotor

Figure 17.- Wake Geometry

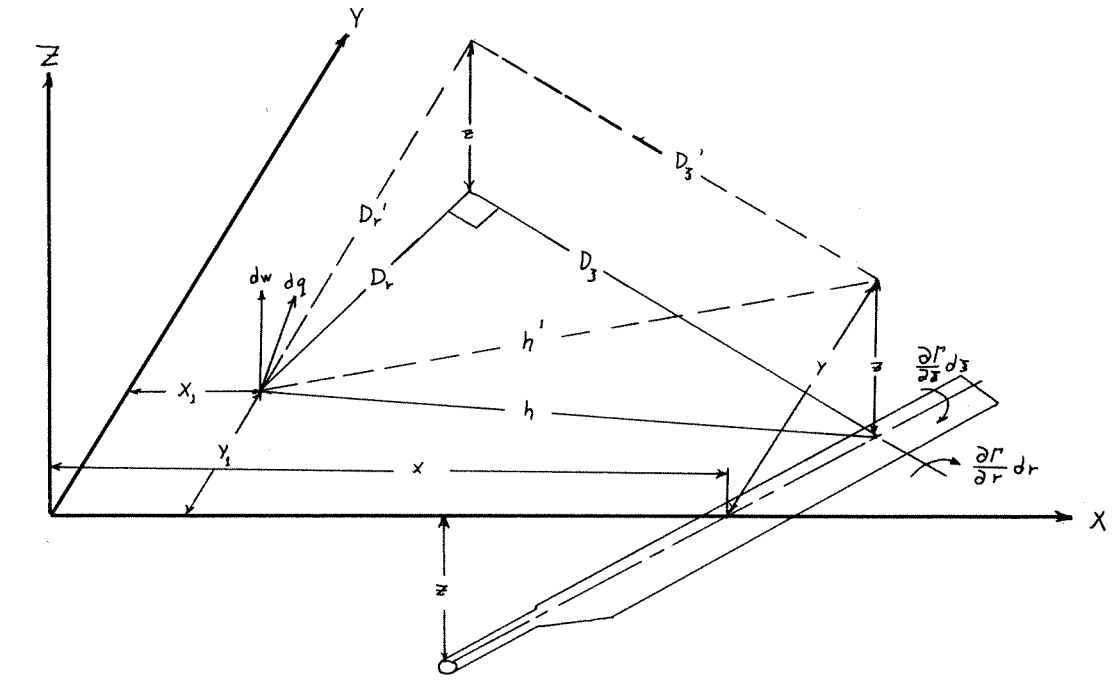

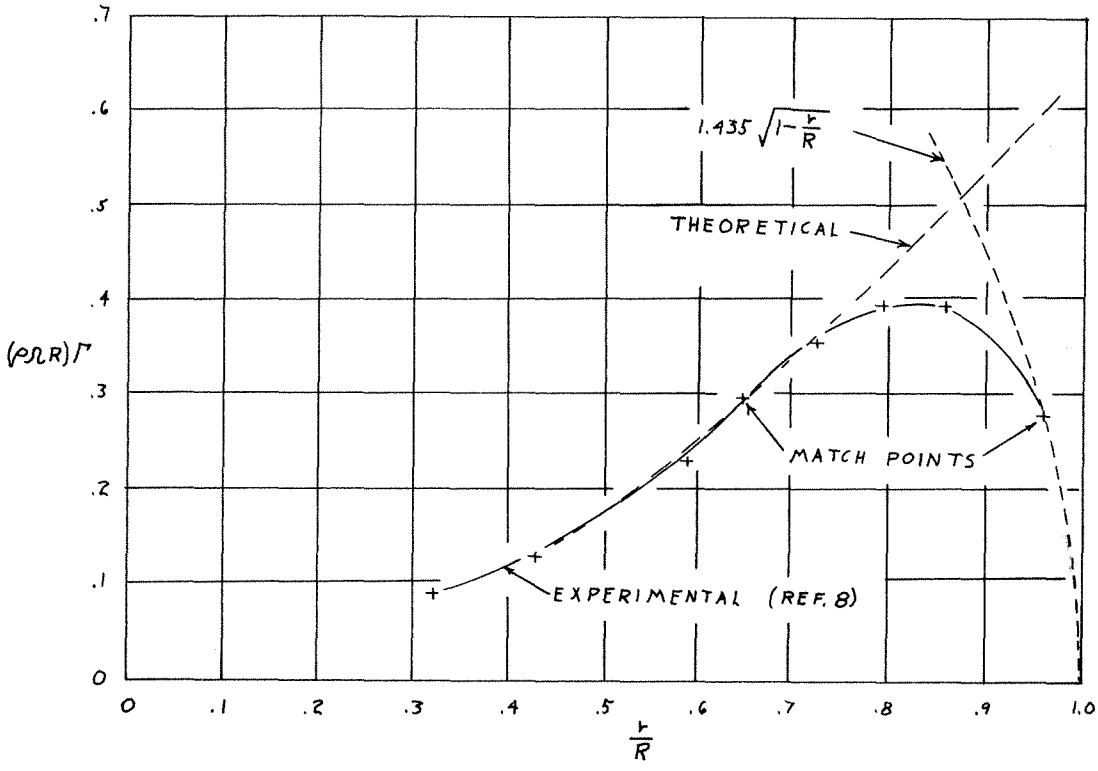

Figure 18a.- Radial Distribution of Circulation

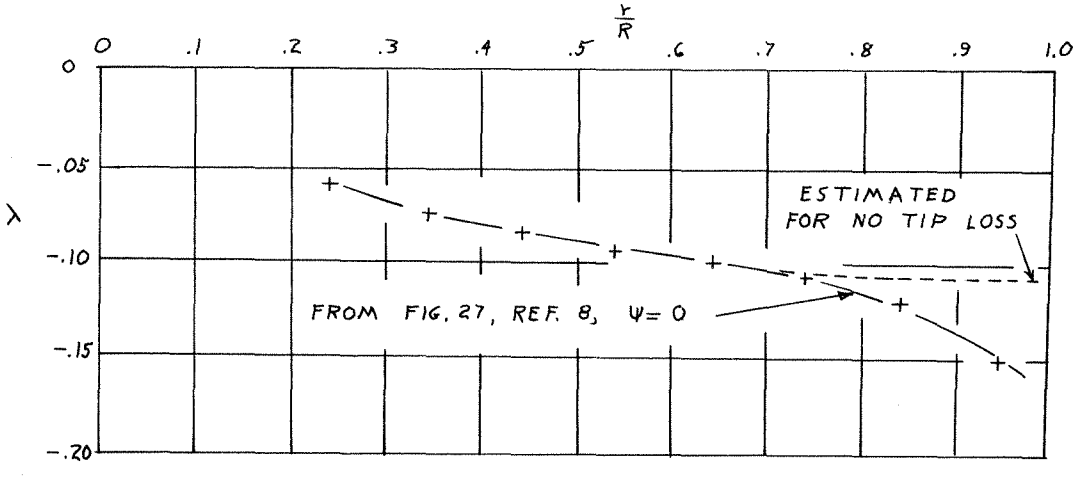

Figure 18b.- Radial Distribution of Inflow Ratio

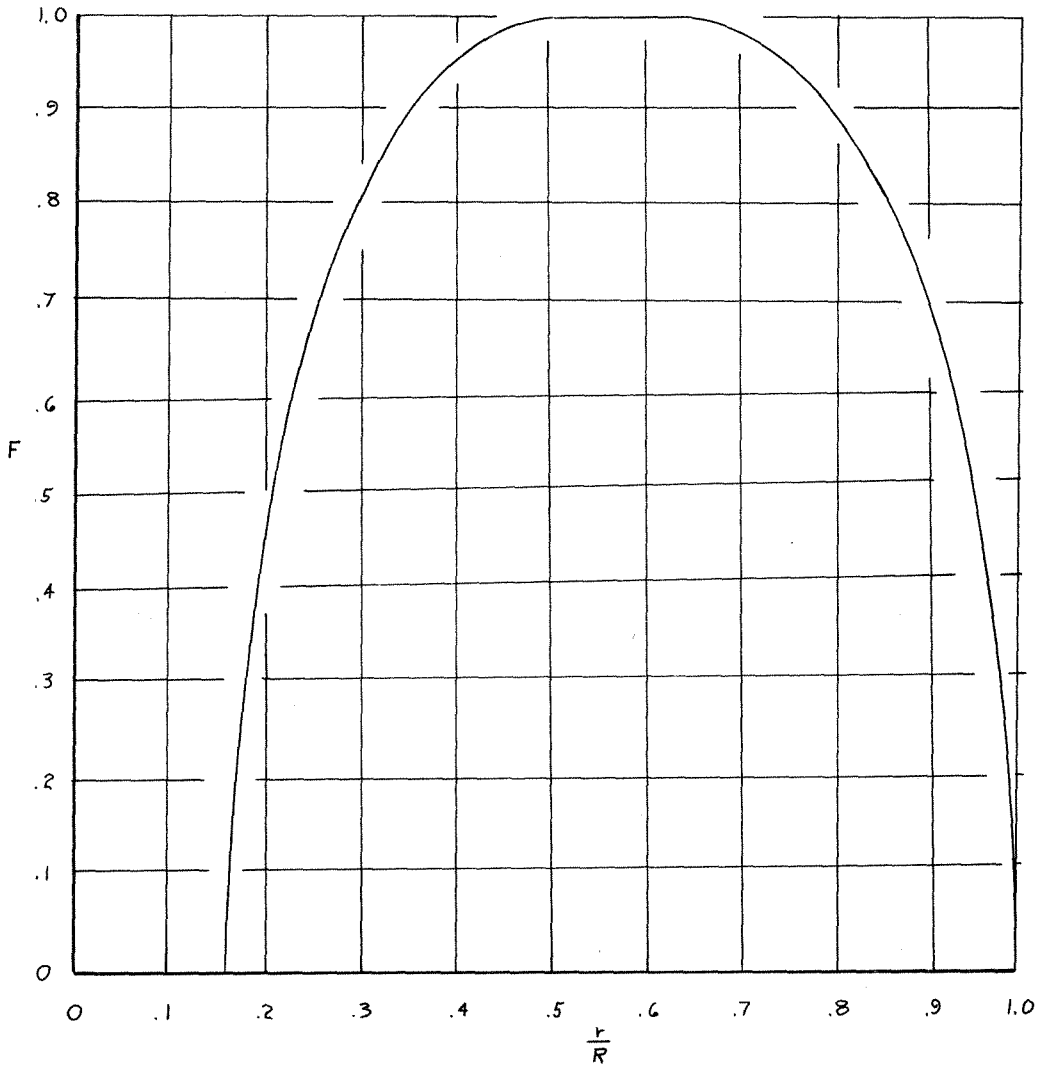

Figure 19.- Tip Loss Function